An extended transcription factor regulatory network involving stabilization loops controls hepatocyte identity

Julie Dubois-Chevalier, Céline Gheeraert, Alexandre Berthier, Clémence Boulet, Vanessa Dubois, Loïc Guille, Marie Fourcot, Guillemette Marot, Karine Gauthier, Laurent Dubuquoy, et al.

An extended transcription factor regulatory network involving stabilization loops controls hepatocyte identity

Running title: Hepatocyte identity stabilization loops

Julie Dubois-Chevalier [1], Céline Gheeraert [1], Alexandre Berthier [1], Clémence Boulet [1], Vanessa Dubois [1,2], Loïc Guille [1], Marie Fourcot [3], Guillemette Marot [4], Karine Gauthier [5], Laurent Dubuquoy [6], Bart Staels [1], Philippe Lefebvre [1,*], Jérôme Eeckhoute [1,*,#]

[1] Univ. Lille, Inserm, CHU Lille, Institut Pasteur de Lille, U1011-EGID, F-59000 Lille, France

[2] Basic and Translational Endocrinology (BaTE), Department of Basic and Applied Medical Sciences, Ghent University, B-9000, Ghent, Belgium

[3] Univ. Lille, CNRS, Inserm, CHU Lille, Institut Pasteur de Lille, US 41 - UAR 2014 - PLBS, F-59000 Lille, France

[4] Univ. Lille, Inria, CHU Lille, ULR 2694 - METRICS : Évaluation des technologies de santé et des pratiques médicales, F-59000 Lille, France

[5] Institut de Génomique Fonctionnelle de Lyon (IGFL), CNRS UMR 5242, INRAE USC 1370, École Normale Supérieure de Lyon, Lyon, France

[6] Univ. Lille, Inserm, CHU Lille, U1286 - INFINITE - Institute for Translational Research in Inflammation, F-59000, Lille, France

[*] Contributed equally

[#] Corresponding author

Corresponding author:

Dr. Jérôme Eeckhoute

INSERM UMR 1011-Bâtiment J&K

Université de Lille, Faculté de Médecine de Lille-Pôle Recherche

Boulevard du Professeur Leclerc

59045 Lille cedex

France

Tel : 33(0)3 20 97 42 20 / Fax : 33(0)3 20 97 42 01

E-mail: jerome.eeckhoute@inserm.fr

ABSTRACT

Cell identity is specified by a core transcriptional regulatory circuitry (CoRC), typically limited to a small set of interconnected cell-specific transcription factors (TFs). By mining global hepatic TF regulons, we provide a more complex organization of the transcriptional regulatory network controlling identity. We have identified that tight functional interconnections controlling hepatocyte identity extend to non-cell-specific TFs beyond the CoRC, which we call hepatocyte identity (Hep-ID)^{CONNECT} TFs. Besides controlling identity effector genes, Hep-ID^{CONNECT} TFs also engage in reciprocal transcriptional regulation with TFs of the CoRC. In homeostatic basal condition, this translates into Hep-ID^{CONNECT} TFs being involved in fine tuning CoRC TF expression including their rhythmic expression patterns. Importantly, a role for Hep-ID^{CONNECT} TFs in the control of hepatocyte identity was revealed in dedifferentiated hepatocytes where Hep-ID^{CONNECT} TFs were able to reset CoRC TF expression. This was observed upon activation of NR1H3 or THRB in hepatocarcinoma or hepatocytes subjected to inflammation-induced loss of identity. Hence, our study establishes that hepatocyte identity is controlled by an extended array of TFs beyond the CoRC uncovering identity stabilization loops.

Keywords: transcription factors / cell identity / core regulatory network / hepatocyte dedifferentiation / liver disease.

INTRODUCTION

Multicellular organisms are built upon collaborative activities of phenotypically and functionally distinct cell-types. Individual cell identities and functions are acquired thanks to the activity of cell-specific transcription factors (TFs). Indeed, cell-specific TFs directly control the expression of non-TF genes exerting activities/functions characterizing individual cell-types, alternatively known as identity effector genes (Almeida *et al*, 2021; Arendt *et al*, 2016). A limited set of identity TFs engaging into auto- and cross-regulatory loops typically defines the core transcriptional regulatory circuitry (CoRC) (Almeida *et al.*, 2021; Arendt *et al.*, 2016). CoRCs are considered cornerstones for establishment and maintenance of cell identities (Almeida *et al.*, 2021; Arendt *et al.*, 2016). Indeed, CoRCs allows to self-sustain high expression of identity TFs and their target effector genes in addition to being involved in the continuous modulation of the hepatic transcriptome in response to environmental stimuli (Almeida *et al.*, 2021; Arendt *et al.*, 2016; Boyer *et al*, 2005; Wilkinson *et al*, 2017).

In line, hepatocyte identity is typically defined as relying on a handful of interconnected hepatocyte-specific CoRC TFs (hereafter called Hep-ID TFs) including HNF4A, FOXA or NR1H4 (FXR) (Tachmatzidi *et al*, 2021). However, many additional TFs beyond these hepatic identity CoRC TFs have been ascribed with roles in the control of hepatocyte activities (Bideyan *et al*, 2021). However, whether and how these additional TFs exert their functions in concert with the hepatic CoRC is not fully understood. Moreover, considering that sustained expression of Hep-ID TFs has a positive impact on hepatic pathological conditions (Berasain *et al*, 2022), better defining how CoRC TFs are functionally linked to additional TFs is of pathophysiological interest. Indeed, breakdown in liver functions in advanced stages of liver injuries and in cancer results from hepatocyte loss of identity stemming from compromised expression of the hepatic CoRC TFs (Berasain *et al.*, 2022; Dubois *et al*, 2020a).

As outlined hereabove, apprehending the transcriptional regulation of cell identity through the lens of CoRCs, by definition, only leads to consider the role of a very limited subset of TFs. In this context, the real architecture and outline of the hepatocyte identity TF network has not been clearly established beyond Hep-ID TFs. We postulated that focusing on TF interconnections at the genomic-scale would allow to define how the Hep-ID TF network spreads beyond the CoRC and would refine our understanding of hepatocyte identity transcriptional control.

RESULTS

Hepatocyte identity TFs extensively co-bind TF-encoding gene promoters beyond the CoRC

We defined the hepatocyte CoRC as a set of 13 Hep-ID TFs commonly defined in different studies as interconnected hepatocyte-specific TFs (D'Alessio *et al*, 2015; Dubois *et al.*, 2020a; Kyrmizi *et al*, 2006; Zhou *et al*, 2017) (Table S1). Hep-ID TFs comprise the well-accepted and thoroughly experimentally-verified drivers of hepatocyte identity (Reizel *et al*, 2020; Tachmatzidi *et al.*, 2021). As expected from our previous studies (Dubois-Chevalier *et al*, 2020; Dubois-Chevalier *et al*, 2017b; Dubois *et al.*, 2020a), monitoring the mouse liver cistromes of 8 Hep-ID TFs (CEBPA, FOXA2, HNF4A, NR1H4, NR5A2, ONECUT1, PPARA, PROX1; Table S2) pointed to their extensive co-recruitment at the Hep-ID TF-encoding gene promoters when compared to a control set of non-Hep-ID TF-encoding gene promoters (Fig.1A and Fig.S1A-B). This led us to define a strategy called Promoter-centric TF network analysis (ProTFnet) (Fig.1B) with the aim to establish global TF interconnections through promoter binding patterns. Indeed, this approach consists in mining TF cistromes to identify TF binding to all TF-encoding gene promoters. Here, hepatic TF cistromes (n=49; including those of Hep-ID TFs and extending to transcriptional cofactors) (Dubois-Chevalier

et al., 2017b; Dubois *et al.*, 2020a) were used to monitor the binding to all TF-encoding gene promoters active in the mouse liver (n=925; see Materials and Methods for details). These promoters were grouped together based on their TF binding pattern similarity, i.e. cistromic-based classification, using a self-organizing map (SOM) (Fig.S2) (Dubois-Chevalier *et al*, 2017a). Hierarchical clustering was next performed and identified 7 main clusters of TF-encoding gene promoters (Fig.1C and Fig.S3A). We annotated these clusters A to G based on progressive TF co-recruitment pattern complexity (Fig.1C-D, Fig.S3B-C and Fig.S4). Promoters from cluster G were also overall the most strongly active as revealed by chromatin accessibility (DHS), hepatic histone acetylation (H3K27ac) or mRNA expression levels of associated TF-encoding genes (Fig.1E and Fig.S5). Moreover, Hep-ID TF binding was also most pronounced at promoters from cluster G, both when considered individually (Fig.S3D-E and Fig.S4G) or collectively, i.e. Hep-ID TF co-recruitment (Fig.1F). Therefore, these data indicated that cluster G captured most of the TF-encoding gene promoters preferentially targeted by Hep-ID TFs.

In order to further characterize TF-encoding genes from cluster G, we prepared an additional classification of TF-encoding gene promoters based on their levels of hepatic activity and specificity [hereafter referred to as promoter hepatic activity score; see Materials and Methods for a full description of how this score was obtained]. This second classification, which was used to discriminate 7 promoter classes (denoted 1 to 7) displaying a progressive increase in the promoter hepatic activity score (Fig.S6; Table S1), was compared with the previously obtained cistromic-based classification. This analysis confirmed that cluster G overall comprised promoters with the highest hepatic activity scores (Fig.1G) including, in particular, a group of promoters shared with class 7 (G-7 promoters, n=13; Fig.S7A-C). G-7 promoters both displayed enrichment for Hep-ID TF-encoding genes (Fig.1H) and were strongly bound by these Hep-ID TFs (Fig.1I and Fig.S7D-F). Hence, G-7 is the prominent

subset of promoters capturing hepatic CoRC auto-/cross-binding. However, in addition to Hep-ID TFs, cluster G also comprised a majority of TF promoters with lower hepatic activity scores (G-4 to G-6 promoters, n=117) (Fig.1G and Fig.S7A-D; Table S1). To further characterize the TF-encoding gene heterogeneity in cluster G, we performed a meta-analysis of transcriptomic data from primary human and mouse cells (n=126 and 39 different cell-types including hepatocytes, respectively) to define 3 groups of TFs displaying cell-type specific (CTS), cell-type enriched (CTE) or ubiquitous (UBQ) expression patterns (Fig.1J and Fig.S8; see Materials and Methods). This further highlighted that, besides Hep-ID TFs and an additional set of cell-specific TFs with well characterized hepatic functions (*Nr1i3*/*Car*, *Rorc*/*Rorg*, *Hnf1a* and *Gata4*) (Tachmatzidi *et al.*, 2021), the majority of TFs from cluster G belonged to CTE or UBQ TFs (Fig.1K and Table S1).

Altogether, these analyses indicated that extensive co-recruitment of Hep-ID TFs is not limited to their own highly hepatocyte-specific genes within the CoRC but extends to an additional set of TFs.

Hep-ID^{CONNECT} TFs are expressed under the control of and collaborate with Hep-ID TFs in the regulation of hepatocyte identity effector genes

In order to further characterize the CTE/UBQ TFs from cluster G, we refined our analysis of their individual expression patterns by defining how their levels of expression in mouse primary hepatocytes (MPH) compare to those in other primary cells (n=38 different cell-types). Interestingly, we found that a subset of the CTE/UBQ TFs from cluster G, hereafter called Hep-ID^{CONNECT} TFs, was nevertheless characterized by privileged hepatocyte expression (i.e. MPH ranked among the top 10 expressing cells and expression in MPH above average expression in other cells) (Fig.2A and Fig.S9). These data suggested that Hep-ID^{CONNECT} TFs might be directly dependent upon Hep-ID TFs for their enhanced hepatocyte expression. In line, expression of Hep-ID^{CONNECT} TFs was decreased in transcriptomic data

obtained from MPH of adult mice with hepatocyte-specific deletion of the Hep-ID TF *Hnf4a* (Fig.2B). Moreover, reminiscent of Hep-ID TF-encoding genes, expression of Hep-ID^{CONNECT} TFs was increased in the final hepatocyte differentiation stage occurring during liver postnatal maturation (Fig.2C). We and others have established that compromised hepatocyte identity due to decreased Hep-ID TF gene expression is commonly found in severe liver injuries in both mouse models and humans (Argemi *et al*, 2019; Berasain *et al.*, 2022; Bou Saleh *et al*, 2021; Dubois *et al.*, 2020a; Gunewardena *et al*, 2022; Hyun *et al*, 2020; Loft *et al*, 2021). Therefore, we further mined Hep-ID^{CONNECT} TF expression in a meta-analysis of transcriptomic data obtained from mouse liver injury models triggering hepatocyte dedifferentiation (Fig.S10). Interestingly, we found that Hep-ID^{CONNECT} TFs showed reduced expression levels in the livers of these mouse models (Fig.2D). Similar observations were made using transcriptomic data obtained from microdissected hepatocytes from alcohol-related human liver cirrhosis (Bou Saleh *et al.*, 2021) (Fig.2E). Overall, observed changes in expression of Hep-ID^{CONNECT} TFs were reminiscent of those of Hep-ID TFs, albeit often with a lower amplitude, and different from those of other TFs from cluster G. A similar observation was made when interrogating the breadth of H3K4me3 labelling at Hep-ID^{CONNECT} TF gene promoters, a feature positively linked to the role of TFs in the control of cell identity (Benayoun *et al*, 2014; Chen *et al*, 2015; Pekowska *et al*, 2010). Indeed, the breadth of H3K4me3 labelling at the promoters of Hep-ID^{CONNECT} TF genes was also comprised in between that observed for the Hep-ID TF and other TF-encoding genes (Fig.2F). Moreover, H3K4me3 labelling at Hep-ID^{CONNECT} TF genes displayed intermediate tissue-specificity when compared to Hep-ID TF genes, on the one hand, and remaining TF-encoding genes from cluster G, on the other hand (Fig S11). Altogether, these data point to the potential importance of Hep-ID^{CONNECT} TFs in fully differentiated hepatocytes.

Indeed, many Hep-ID^{CONNECT} TFs have individually, i.e. without an identified unifying rationale, been ascribed, at least to some extent, a role in the control of hepatic metabolic activities (Fig.S12). In line, mining genes associated with phenotypes from the Mammalian Phenotype Ontology resource (Chen *et al*, 2007; Smith *et al*, 2005) revealed that, albeit less significant when compared to Hep-ID TFs, Hep-ID^{CONNECT} TF-encoding genes are linked to abnormal liver phenotypes and metabolic functions (Fig.2G). Mining transcriptomic data obtained from the livers of mice with hepatocyte-specific deletion of individual Hep-ID^{CONNECT} TF-encoding genes (hep-/- mice) indicated that this is functionally underlain by a preferential dysregulation of downstream hepatocyte identity effector genes, i.e. non-TF genes with liver-specific broad H3K4me3 domains defined in (Dubois *et al.*, 2020a) (Fig.2H). While such a bias was also observed in transcriptomic data obtained from the livers of mice deficient for individual Hep-ID TF genes, deletion of the general chromatin organizer *Ctcf* did not give rise to preferential dysregulation of hepatocyte identity effector genes (Fig.2H). In line, similar to Hep-ID TFs and different from CTCF, binding of most Hep-ID^{CONNECT} TFs was stronger at hepatocyte identity effector gene promoters (Fig.2I). We found that preferential binding remained observable when using a more stringent control, i.e. promoters with comparable accessibility and activity (Activity matched control promoters; see Materials and Methods and Fig.S13 for further details). This ruled out that chromatin accessibility alone explains preferential binding to Hep-ID TF gene promoters (Fig.2I). Finally, binding of Hep-ID and Hep-ID^{CONNECT} TFs correlated at the promoter of these genes pointing to combinatorial transcriptional regulation (Fig.2J).

Altogether, these data identified that Hep-ID TFs of the hepatic CoRC target Hep-ID^{CONNECT} TF genes, and that these 2 sets of TFs further collaborate to control identity effector genes.

Hep-ID^{CONNECT} TFs are reciprocally targeting Hep-ID TF-encoding genes to finely tune their expression in homeostatic conditions

We hypothesized that the intimate connection between Hep-ID and Hep-ID^{CONNECT} TFs identified so far could further extend to reciprocal transcriptional regulation where Hep-ID^{CONNECT} TFs would bind and control expression of Hep-ID TF-encoding genes. Mining Hep-ID^{CONNECT} TFs binding in mouse liver indicated greater recruitment to Hep-ID TF gene promoters when compared to control activity-matched TF-encoding gene promoters, reminiscent of data obtained for Hep-ID TFs (Fig.3A and Fig.S14). However, this only translated into moderate transcriptional changes in expression of Hep-ID TF-encoding genes. Indeed, only the deletion of a subset of the Hep-ID TF-encoding genes, and not that of Hep-ID^{CONNECT} TF genes, individually triggers global down-regulation of the Hep-ID TF gene expression (Fig.3B). This most probably relates to the intrinsic role of identity TF networks, which are built-up to allow robustness of individual cell-type transcriptional programs (Almeida *et al.*, 2021; Kyrmizi *et al.*, 2006).

Severeal Hep-ID^{CONNECT} TFs are central to establishment of rhythmic hepatocyte gene expression (Fig.S15) including both circadian (BHLHE40, CLOCK, DBP, NFIL3, NR1D1/2) (Mukherji *et al*, 2019) and ultradian (XBP1) (Meng *et al*, 2020; Pan *et al*, 2020) rhythms. Hence, rather than being instrumental for regulating steady-state expression levels of Hep-ID TF genes, we envisioned that Hep-ID^{CONNECT} TFs might be involved in proper rhythmic expression of Hep-ID TF encoding genes. In line, mining data from (Meng *et al.*, 2020) revealed that a majority of Hep-ID TF genes (9 out of 13), including for example *Mlxipl*, were characterized by XBP-1 dependent ultradian expression patterns (Fig.3C-D and Table S3).

Activation of Hep-ID^{CONNECT} TFs resets CoRC TF expression and hepatocyte identity in dedifferentiated hepatocytes

Recent studies have found that individual TF activities may only be fully revealed in non-basal conditions and that TFs may be important to (re-)establish rather than to maintain cell-specific transcriptomes (Hunter *et al*, 2020; Lo *et al*, 2022). Therefore, we envisioned that, at least for some Hep-ID^{CONNECT} TFs, a role in controlling the Hep-ID TF network might be revealed in a biological context where hepatocyte identity is challenged such as cancer. Mining transcriptomics of human hepatocarcinoma (HCC) from the cancer genome atlas (TCGA; n=366) indicated that expression of Hep-ID TF genes exhibited a trend towards positive correlation with that of many Hep-ID^{CONNECT} TFs (Fig.4A). Moreover, binging of Hep-ID^{CONNECT} TFs to Hep-ID TF genes was also observed in hepatic cancer cells (Fig.4B) and overexpression or activation of several Hep-ID^{CONNECT} TFs, GATA binding protein 6 (GATA6), krüppel-like factor 9 (KLF9), T-box transcription factor 3 (TBX3) and the nuclear receptors liver X receptor alpha (NR1H3 also known as LXR alpha) and thyroid hormone receptor beta (THRB), has been shown to opposite hepatocarcinogenesis (Fig4A) (Kowalik *et al*, 2020; Liang *et al*, 2021; Lin *et al*, 2020; Sun *et al*, 2014; Tan *et al*, 2019). Mechanisms involved have largely remained undefined and we hypothesized that these HCC suppressive effects may be linked to a resetting of Hep-ID TF expression. Therefore, we leveraged transcriptomic analyses performed on HCC cell-lines treated with ligands activating NR1H3 (Huh7 cells treated with GW3965) (Vazquez Salgado *et al*, 2022) or THRB (HepG2 cells treated with 3,3′,5-triiodo-L-thyronine (T3) or GC-1) (Yuan *et al*, 2012). In line with our hypothesis, we found that treatment with GW3965, T3 or GC-1 induced a global increase in Hep-ID TF gene expression in HCC cell-lines (Fig.4C). We were able to reproduce induction of Hep-ID TF gene expression by T3 and GC-1 in HepG2 cells, induction of *DIO1* being used as a positive control in these assays (Fig.4D-E). In addition, THRB activation also increased the ratio of HNF4A adult promoter P1- to embryonic promoter P2-derived isoforms (Fig.4F), a phenomenon known to promote hepatocyte differentiation and function (Dubois *et al*,

2020b). Western blot assays confirmed T3-induced changes in Hep-ID TF levels (Fig.4G). Similar data were obtained using a non-cancerous human immortalized hepatic cell-line (IHH) used as another model of partially dedifferentiated hepatocytes (Schippers *et al*, 1997a) (Fig.S16). Moreover, interrogating the transcriptomic data obtained in a rat model of hepatocarcinogenesis (Kowalik *et al.*, 2020) revealed that T3 was able to counteract the cancer-driven loss of expression of Hep-ID TFs (Fig.4H). Indeed, T3 treatment led to robust transcriptional induction of Hep-ID TF-encoding genes whose expression was most strongly down-regulated in the cancerous nodules (Fig.4I). This was in contrast with T3 not triggering a global rise in Hep-ID TF expression in healthy mice (Fig.S17) (Singh *et al*, 2018) further substantiating a role for THRB in controlling Hep-ID TF genes only in context of dedifferentiated hepatocytes. T3-mediated re-expression of Hep-ID TFs further translated into re-expression of the most strongly downregulated identity effector genes consistent with concomitant re-establishment of a transcriptional program closer to that of differentiated hepatocytes (Fig.4J).

Beyond cancer, as stated earlier, we and others have reported that hepatocyte partial loss of identity is a hallmark of severe liver injuries [recently reviewed in (Berasain *et al.*, 2022)]. In particular, inflammation is a well-established common driver of hepatocyte dysfunction (Del Campo *et al*, 2018). For instance, tumor necrosis factor or interleukin 1 beta (IL1B) have been shown to trigger loss of hepatocyte identity (Hyun *et al.*, 2020). In this context, we set-up an experimental model where mice were injected with IL1B for 3h before livers were collected. IL1B treatment indeed triggered loss of hepatocyte identity including decreased expression of several Hep-ID TF genes as assessed through transcriptomic analyses (Fig.S18A-B). We next determined whether T3 treatment promoted the recovery of Hep-ID TF gene expression in this model, i.e. mice were first injected with IL1B and 3h latter with or without T3 for an additional 3h (Fig.5A). This acute setting allowed us to investigate the

effect of T3 independent of its previously described pro-regenerative activities through modulation of hepatocyte proliferation (Tang *et al*, 2022). Inbred laboratory mice raised in standardized conditions nevertheless keep displaying high phenotypic trait variability (Gartner, 1990; Tuttle *et al*, 2018) and are prone to polyphenism, i.e several discrete phenotypes on the same genetic background (Dalgaard *et al*, 2016; Yang *et al*, 2022). Here, mice were subdivided into 3 groups (low, intermediate and high responsiveness groups) based on their response to T3 as judged using stimulation of the *Dio1* and *Hectd3* gene expression, which are previously identified THRB hepatic target genes (Fig.5B) (Paquette *et al*, 2011). Importantly, these differences were due to variability in the T3 response only, since IL1B-mediated induction of pro-inflammatory genes was similar between the 3 groups and no negative correlation between T3 and IL1B responses was detected (Fig.5C and Fig.S17C). Interestingly, the IL1B+T3 high responsiveness group showed expression recovery of Hep-ID TF genes whose levels were higher in this group when compared to those in the IL1B only and/or IL1B+T3 low responsiveness groups (Fig.5D).

Altogether, these data have identified the Hep-ID^{CONNECT} TF THRB as an actionable target to reset expression of hepatic identity TF genes in partially dedifferentiated hepatocytes.

DISCUSSION

Our promoter-centric and multi-omics approach called ProTFnet allowed us to unveil the complexity of the TF network controlling hepatocyte identity and functions. Using this approach, we identified that Hep-ID TFs of the CoRC are tightly connected with an additional layer of TFs through reciprocal co-recruitment to their promoters. The CoRC, in addition to being instrumental for cell identity establishment and maintenance, comprises TFs which are also key for controlling and adapting mature cell functions to homeostatic requirements. In

this context, the tight connection between Hep-ID^{CONNECT} TFs and the CoRC provides an additional layer of regulation to finely tune Hep-ID TF expression. For instance, Hep-ID^{CONNECT} TFs comprise regulators of rhythmic gene expression including XBP1. Other Hep-ID^{CONNECT} TFs, TBX3 and TCF7L2, have been identified as regulators of zonated hepatocyte transcriptional programs (González-Blas *et al*, 2022) pointing to a role of Hep-ID^{CONNECT} TFs in specifying proper hepatic gene expression in both space and time. Importantly, ryhtmic and zonated hepatic gene expression are crucial to maintain appropriate liver metabolic and non-metabolic activities (Meng *et al.*, 2020; Mukherji *et al.*, 2019; Pan *et al.*, 2020; Paris & Henderson, 2022).

While not being required to sustain Hep-ID TF gene expression and cell identity in basal condition, our data obtained with NR1H3 and THRB in dedifferentiated hepatocytes revealed that Hep-ID^{CONNECT} TF activation can be leveraged to reset the CoRC and hepatocyte identity. These findings are consistent with other recent observations where TF binding to cell-specific target genes translates into a more critical role in (re)establishment and dynamic regulation rather than maintenance of steady-state gene expression levels (Lo *et al.*, 2022). Our study is also consistent with recent insights into the understanding of cell fate choice, which have suggested a more distributed form of control relying on combinatorial activities of dozens of TFs rather than an organization strictly dominated by a few master TFs (Chubb *et al*, 2021; Mittnenzweig *et al*, 2021). In this context, we propose that Hep-ID^{CONNECT} TFs are involved in identity stabilization loops, whose functional importance with regards to cell identity is revealed in pathophysiological situations of dedifferentiation (Fig.6). Context-dependent activities is an intrinsic property of TFs and precisely defining how Hep-ID^{CONNECT} TFs sense the cellular state to adapt their functions will require additional studies.

Loss of hepatocyte identity is a main feature of tumorigenesis, but is now ascribed a broader pathophysiological relevance including loss of activity of severely injured livers

(Berasain *et al.*, 2022). In both situations, resetting hepatocyte identity through re-expression of CoRC TFs is considered of potential therapeutic interest (Berasain *et al.*, 2022; Chao *et al*, 2020). By identifying the Hep-ID^{CONNECT} TF-controlled identity stabilization loops, our study has identified new avenues to achieve this goal. In particular, our data with agonists of the nuclear receptors NR1H3 and THRB are particularly relevant as several of those are being considered for treatment of liver diseases (Hatziagelaki *et al*, 2022; Russo-Savage & Schulman, 2021). With regards to HCC, our data provide explanation for the reported beneficial effects exerted by NR1H3 and THRB. Many Hep-ID^{CONNECT} TFs, including NR1H3 and THRB, do not display typically used features to define hepatocyte identity TFs such as hepatocyte-specific expression and association with super-enhancers (Dubois *et al.*, 2020a; Hnisz *et al*, 2013) (Table S4). Hence, our study has allowed to uncover an unforeseen role for an extended transcriptional regulatory network beyond the CoRC in the control of hepatocyte identity (Fig.6).

MATERIALS AND METHODS

Data retrieval

Public functional genomics data used in this study were downloaded from the Gene Expression Omnibus (GEO) (Barrett *et al*, 2013), ArrayExpress (Sarkans *et al*, 2021), ENCODE (Yue et al. 2014), the UCSC Genome Browser (Raney et al. 2011), FANTOM5 (Lizio *et al*, 2015) or from BioGPS (Wu et al. 2009) and are listed in Table S2.

Hep-ID TFs were defined as hepatocyte-identity TFs retrieved in at least 2 out of 3 independent studies (D'Alessio *et al.*, 2015; Dubois *et al.*, 2020a; Zhou *et al.*, 2017). The top 20 TFs were used for (D'Alessio *et al.*, 2015).

Mouse liver active promoters were defined based on Precision nuclear Run-On Sequencing (PRO-Seq) data (Wang *et al*, 2018). HepG2 active promoters were defined as the

transcriptional start sites (TSSs) from Gencode v32 (Frankish *et al*, 2018) with H3K27ac ChIP-seq signal (ENCODE, Table S2) with at least 2-fold enrichment over control within a 1 kilobase (+/- 500 bp of TSS) window. Only the most active TSS per gene, i.e. highest H3K27ac ChIP-seq signal, were kept.

The IDR thresholded peaks issued from ChIP-seq analyses of flag-tagged Hep-ID^{CONNECT} TFs (n=14) in HepG2 cells were obtained from ENCODE (Table S2).

Tau indexes of tissue-specific expression were retrieved from (Kryuchkova-Mostacci & Robinson-Rechavi, 2017).

Self-Organizing Maps (SOM) analyses

Active promoters in the mouse liver were defined as *cis*-regulatory modules, i.e. genomic regions bound by at least 2 different transcriptional regulators (Fig.S2A-B) as in (Dubois-Chevalier *et al.*, 2017a), which overlap active TSSs identified as PRO-seq data summits in (Wang *et al.*, 2018). Non-unique associations between TSSs and genes in the PRO-seq data were discarded. Only transcription factor (TF) encoding genes, retrieved using a manually curated gene list originally obtained from the AnimalTFDB2.0 database (Zhang *et al*, 2015), were considered. Transcriptional regulator co-recruitment analyses made use of mouse liver ChIP-seq data for 49 factors (Table S2), which were uniformly processed including quality control checks as described in (Dubois-Chevalier *et al.*, 2017a). All these data were obtained using the liver of untreated adult mice. In line with the vast majority of the liver chromatin stemming from hepatocytes (which are the prominent cell-type in the liver and are, moreover, mostly polyploid cells - up to 85% in mice with mainly tetraploid hepatocytes) (Duncan *et al*, 2010), hepatic TF cistromes can be faithfully inferred from mouse liver ChIP-seq data (Dubois-Chevalier *et al.*, 2017a; Dubois *et al.*, 2020a; Kyrmizi *et al.*, 2006; Schmidt *et al*, 2010; Sommars *et al*, 2019).

The SOM were generated using the R package kohonen2 (Wehrens & Buydens, 2007) as described in (Dubois-Chevalier *et al.*, 2017a). Cells containing promoters with similar transcriptional regulator binding patterns (Fig.S2C-D) were further grouped into clusters (denoted A-G) based on hierarchical clustering performed using the hclust function of the R package Stats (R_Core_Team, 2015). We used the Ward agglomeration method and the best representative transcriptional regulator combination (prototype) for each individual cell. The number of clusters was chosen according to homogeneity analyses (http://lastresortsoftware.blogspot.fr/2010/08/homogeneity-analysis-of-hierarchical.html) (Bedward *et al*, 1992) and biological significance. A planar projection of the toroidal map was used for data visualization.

Analyses of transcriptional regulator co-recruitment patterns in SOM-derived clusters

Transcriptional regulator co-occurrence in clusters A-G was used to calculate Tanimoto distance matrices, which were used to draw heatmaps and perform hierarchical clustering or perform multi-dimensionnal scaling (MDS) analyses using R (R_Core_Team, 2015) as described in (Dubois-Chevalier *et al.*, 2017a). To analyze the combinations of transcriptional regulators bound at the different promoters of a given cluster, a "frequent itemsets" search (combinations of 2 to 49 regulators) was performed using the arules R package (Hahsler *et al*, 2005). Only itemsets occurring in at least 50% of promoters of a given cluster were considered and defined as the core co-recruitment nodes. Finally, the percentage of occurrence of each transcriptional regulator in these nodes was retrieved.

Transcriptomic data analyses

Processing of raw data and differential gene expression analyses

Raw transcriptomic data from Affymetrix microarrays were normalized on a local instance of Galaxy (Afgan *et al*, 2018) using the GIANT APTtool (Affymetrix Power Tools; www.thermofisher.com/fr/fr/home/life-science/microarray-analysis/microarray-analysis-partners-programs/affymetrix-developers-network/affymetrix-power-tools.html) (with options : gc correction when available, scale intensity and rma at probeset level) from the GIANT toolbox (Vandel *et al*, 2020). Normalized expressions were averaged per Gene Symbol (NetAffx Annotation Release 36, July, 2016). Raw transcriptomic data from Agilent microarrays were processed with the limma R package (Ritchie *et al*, 2015) used to normalize the data through the "backgroundCorrect" function (parameters used were method :"normexp" and normexp.method : "rma") and to filter out low expressed probes. Normalized data from Illumina Bead Chips were retrieved from the Gene Expression Omnibus database and annotated using GPL6101_Illumina_RatRef-12_V1_0_R1_11222119. Orthologous mouse genes were retrieved using Ensembl annotations (release 105) (Howe *et al*, 2021). Differential expression analyses were performed with GIANT using the limma tool (FDR cutoff set at 0.15).

RNA-seq data were analyzed using the Galaxy web platform (Afgan *et al.*, 2018). Mapping of reads on mm10 was performed with HISAT2 (version 2.21; options: default) (Kim *et al*, 2019). Mapped reads mapping to exons were subsequently retrieved and merged by gene_id with Htseq-count (version 0.9.1) (Anders *et al*, 2015) using the mm10 annotation of Ensembl (release 102) (Yates *et al*, 2020) (with the following options, mode: union, minimum alignment quality: 10, "do not count non uniquely or ambiguously mapped reads", stranded: no). Normalization and differential analyses were performed with EdgeR (version 3.36.0) (Liu *et al*, 2015; Robinson *et al*, 2010) (options: lowly expressed genes filtered out, cutoff: <1CPM in n samples - with n corresponding to number of biological replicates in one condition, FDR<0.15, normalization method: TMM, Robust settings: True). Normalized gene

expressions were obtained by averaging data per Gene Symbol using the Ensembl annotation (release 105) (Howe *et al.*, 2021). Dot plots displaying dysregulation in transcriptomic data were performed with the ggplot2 R package (Wickham, 2016).

Mining of CAGE-seq data to define CTS (cell-type specific), CTE (cell-type enriched) and UBQ (ubiquitous) TFs

CAGE-seq data from FANTOM5 (Lizio *et al.*, 2015) were used to define CTS, CTE and UBQ TF-encoding genes based on their patterns of expression in primary human and mouse cells. Human and mouse orthologous genes were defined using the Ensembl annotation (version 105) (Howe *et al.*, 2021). Only TF-encoding genes retrieved in both the human and mouse CAGE-seq data (n=1009) were considered. Their expression levels in mouse and human cells were stacked in a unique matrix centered and scaled, which was used to perform a Multiple Factor Analysis (MFA) using the MFA function of the R package FactoMineR (Lê *et al*, 2008) considering expression in mouse and human cells as two distinct groups of variables and TFs as individuals (parameters were set as follows, type: c('s','s'), ncp: 5). The 2 first components of this MFA accompted for approximately 84% of the variability of the two combined datasets. A hierarchical clustering was performed on these 5 first components using the HCPC function of the FactoMineR package (parameters were set as follows, nbclust: 3, metric: "euclidean", method: "ward"). This identified 3 clusters of TFs characterized by an increasing number of cell-types displaying high expression from CTS to UBQ TFs (Fig.S8).

Mining of transcriptomic data to monitor hepatic dedifferentiation

To monitor hepatocyte dedifferentiation in mouse liver injury models, all liver injury transcriptomic data were batch corrected against the liver development transcriptomic data used as a reference. This was performed with the ComBat function of the R package SVA (parameters were set as follows, mean.only: T, par.prior: T, control samples for the batch

correction were the adult livers for the differentiation study and the livers from wild-type or untreated mice for the injury studies) (Leek *et al*, 2022). Then a principal component analysis (PCA) was computed on the liver differentiation study using the R package FactoMineR (scale.unit set to F) (Lê *et al.*, 2008). Since the first component, representing 64% of the dataset variability, allowed to separate the different stages of liver differentiation, it was used to project the liver injury studies. Fold changes between injured and control livers were computed on the batch corrected data and the median $\log_2$ fold change for individual genes across the different studies was recovered and plotted.

Mining transcriptional changes in identity genes versus control gene sets

Transcriptional modulations of identity effector and TF-encoding genes were compared to those in control genes matched for mouse liver promoter activity. A hierarchical clustering was performed based on promoter DHS-seq and H3K27ac ChIP-seq signals together with mouse liver gene expression levels considering all active non-TF genes (Fig.S13) or only TF-encoding genes (Fig.S14). Individual signals were scaled and clustering was performed using $\log_2$-transformed data. This allowed to define 4 clusters of promoters with different activity levels among both non-TF and TF-encoding genes. Groups of control genes were defined by randomly selecting an equivalent number of non-identity genes matching the distribution of identity effector or TF genes in these clusters. This was performed 1000 times (without replacement) to compare the identity genes to the individual control gene sets (Fig.S13 and Fig.S14). Results of Wilcoxon rank sum tests were recorded and the mode of the p-value distribution was used to select a representative control gene set among the 1000 subsamples. Selected representative control groups were in main figures.

Gene expression correlation in human HCC

The cbBioPortal (https://www.cbioportal.org/) (Gao *et al*, 2013) was used to retrieved spearman correlations between the log2 mRNA expression of individual Hep-ID^{CONNECT} TF

genes with that of Hep-ID TF genes in HCC within "Liver Hepatocellular Carcinoma (TCGA, Firehose Legacy)" (n=366 samples).

DHS-seq and histone ChIP-seq data analyses

Uniform reprocessing of the data including peak calling and genome-wide average signal has been described in (Dubois-Chevalier *et al.*, 2017a). ChIP-seq signals were also alternatively used as enrichments over input, which were obtained as follows. First, input datasets from several mouse liver ChIP-seq studies (Table S2) were merged into a "meta-input" file after removal of duplicated reads and false-positives regions identified by ENCODE (blacklisted regions v1) (Amemiya *et al*, 2019) or defined as repeatedly enriched in inputs and IgG ChIP-seq in our previous study (Dubois-Chevalier *et al.*, 2017a). Then, the Bam file for each TF ChIP-seq dataset was used to run MACS2 callpeak (-g=1.89e9, -q=0.05, --keep-dup=all, --scale-to=small, B) using the "meta-input" Bam file as control. Finally, the two BedGraph files issued from MACS2 callpeak were used in MACS2 bdgcmp (m=logFE) to obtain the genome-wide $\log_2$ fold enrichment track files over input for each TF (MACS2 version 2.2.7.1) (Zhang *et al*, 2008). DHS-seq or ChIP-seq signal at a given promoter was defined as the maximum signal within TF binding sites (i.e. *cis*-regulatory modules as defined hereabove) encompassing this promoter retrieved using the extract bed function of bwtool version 1.0 (Pohl & Beato, 2014). Comparison of individual TF binding to identity and control gene promoters involved reiterative comparisons with independent matched control groups as described hereabove for transcriptomics analyses. Combinatorial binding of Hep-ID TFs, Hep-ID^{CONNECT} and CTCF on effector gene promoters was compared using the distance correlation provided by the dcor function of the Rfast package in R (Papadakis *et al*, 2022).

Visualization of ChIP-seq data at selected genes was performed using the Integrated Genome Browser (IGB 9.1.4) (Freese *et al*, 2016)

H3K4me3 ENCODE ChIP-seq data from mouse tissues (Shen *et al*, 2012) were used to call H3K4me3-enriched regions using the broad peak calling option of MACS2 as described in (Chen *et al.*, 2015). Genes were assigned to H3K4me3-enriched regions using the closestBed function (with parameters -t all, -k 1, -d, -mdb) of the BEDTools version 2.3.0 (Quinlan & Hall, 2010), i.e. active gene TSS from the mouse liver PRO-Seq data (Wang *et al.*, 2018) were assigned H3K4me3-enriched regions when distance was 0. Calling of super-enhancers (SE) and target gene assignation, essentially performed as in (Loven *et al*, 2013; Whyte *et al*, 2013), was previously described (Dubois-Chevalier *et al.*, 2020).

Classification of TFs based on their promoter hepatic activity score

In order to monitor liver specificity, the DHS-seq or H3K27ac ChIP-seq signals were extracted considering a region spanning +/- 500 base pairs around active promoters (summits of PRO-seq data) (Wang *et al.*, 2018). The DHS and H3K27ac signals for each tissue were normalized using the Spark method (Nielsen *et al*, 2012), which takes into account signal median and variance on all genes in a tissue. Liver specificity indexes were computed by dividing the normalized signals in the liver by the average normalized signals in other tissues (Table S2). A gene expression liver specificity index was similarly computed using normalized gene expressions extracted from the BioGPS Mouse MOE430 Gene Atlas (Wu *et al*, 2016) (Table S2). Log_2-transformed signals, gene expressions and liver-specificity indexes were combined in a matrix, which was centered and scaled and further used for hierarchical clustering using the hclust function of R (parameters were set as follows, method: “Ward.D2” on Euclidean distance matrix) (R_Core_Team, 2015). This allowed to define 7 TF-encoding gene promoter classes characterized by increasing liver activity and specificity together referred to as hepatic activity score (Fig.S6). Heatmaps were plotted with heatmap.2 from the gplots R package (Warnes *et al*, 2022).

H3K27ac ChIP-seq data from purified mouse primary hepatocytes *versus* non-hepatocytes (Roh *et al*, 2017) were further used to characterize the obtained clusters. CAGE-seq data from FANTOM5 (Table S2) were also leveraged to calculate gene expression in hepatocytes when compared to average expression in other primary cell-types.

TF-encoding gene promoters were grouped according to both clustering based on transcriptional regulator co-recruitment (clusters A-G) and based on hepatic activity and specificity (classes 1-7).

Hep-ID^{CONNECT} TF binding to Hep-ID TF encoding genes in HepG2 cells

Mouse phenotype ontology and literature mining

Enrichments within the mouse phenotype ontology or biological pathway data were defined using ToppCluster (Chen *et al.*, 2007; Kaimal *et al*, 2010). Default parameters were used and only terms linked to >5 TF-encoding genes were considered.

References to Hep-ID^{CONNECT} TFs in the scientific literature related to liver/hepatocyte metabolic functions were retrieved using the easyPubMed package (https://www.data-pulse.com/dev_site/easypubmed/) in R. Articles with co-occurrence of a given Hep-ID^{CONNECT} TF gene name and ("hepatocyte" or "liver") and "metabolism" in their title or abstract were considered. The number of retrieved manuscripts for each Hep-ID^{CONNECT} TF was visualized as a heatmap prepared using the heatmap.2 function of the R package gplots.

Cell culture and treatments

The human cell line HepG2 (ATCC, HB-8065) was cultured in minimum essential medium (MEM) (Gibco, 11095080) supplemented with 10% fetal bovine serum (FBS;

Dutscher, 500105H1), MEM non-essential amino acids (Gibco, 11140035), 1 mM sodium pyruvate (Gibco, 11360070) and 100 U/mL penicillin-streptomycin (Gibco, 15140). Immortalized human hepatocytes (IHH) (Schippers *et al*, 1997b) were cultured in William's E medium (Gibco, 22551022) supplemented with 10% FBS (Dutscher, SV30160.03), 20 mU/mL bovin insulin (Sigma, I5500), 50 nM dexamethasone (Sigma, D1756) and 100 U/mL penicillin-streptomycin (Gibco, 15140). Cell culture was performed in a humidified atmosphere of 5% CO2 in a 37 °C incubator. Cells were grown in media containing 10% dextran-coated charcoal stripped serum for 48h and then treated with 10 nM T3 (T6397, Sigma-Aldrich) or 10 nM GC-1 (SML1900, Sigma-Aldrich) for 24 or 96h before being harvested for RNA or protein extraction. For serum stripping, activated charcaol solution (C9157, Sigma-Aldrich) was washed 3 times and prepared in ultra-pure water at final concentration 5%. Dextran T70 (2.5g ; 31390, Sigma-Aldrich) was added to the pellet and charcoal-coated dextran was mixed with 500 mL of serum and incubated overnight at 4°C. After centrifugation (20 min, 4000g, room temperature), the serum was filtered using a 0.2 µm filter and heat inactivated at 56°C for 45 min.

Mouse experiments

Young adult male C57BL/6J wild-type (WT) mice (7-11 weeks old) were purchased from Charles River and housed in standard cages in a temperature-controlled room (22–24°C) with a 12-h dark–light cycle. They had *ad libitum* access to tap water and standard chow and were allowed to acclimate for 2 weeks prior to initiation of the experimental protocol. Acute liver inflammation was induced by intraperitoneal injection of recombinant mouse IL1B using 0.5 µg/ mouse (575102, BioLegend) or vehicle (PBS) for 3h followed by T3 treatment 0.2 mpk (T6397, Sigma-Aldrich). Livers were collected 3h later. Mice with hepatocyte-specific deletion of *Thrb* have been described in (Billon *et al*, 2014).

All animal studies were performed in compliance with EU specifications regarding the use of laboratory animals and have been approved by the Nord-Pas de Calais Ethical Committee (APAFIS#30322-202102221656794 v4).

RNA expression analyses

Tissues were homogenized using Minilys and 1.4 mm ceramic beads (Bertin Technologies). Total RNA was extracted from cell lines and tissues using the Nucleospin® RNA kit (Macherey-Nagel) according to the manufacturer's protocol.

RNA was reverse-transcribed using the High-Capacity cDNA Reverse Transcription Kit (Applied Biosystem). Quantitative PCR (qPCR) was performed on an Fast Applied (Applied Biosystem, Life Technologies, Cergy Pontoise, France) using the Takyon kit (Agilent Technologies). The specificity of the amplification was checked by recording the dissociation curves, and the efficiency was verified to be above 95% for each primer pair. mRNA levels were normalized to the expression of housekeeping genes and the fold induction was calculated using the cycle threshold (ΔΔCT) method. The sequences of primers used are listed in Table S5.

For transcriptomic analyses, RNA integrity and quantity were evaluated using the Agilent 2100 Bioanalyser (Agilent Technologies). RNA was then processed for transcriptomic analysis using Affymetrix GeneChip arrays (MoGene 2.0) or high-throughput sequencing (RNA-seq) as previously described (Bobowski-Gerard *et al*, 2022).

Protein extraction

Proteins from the chromatin fraction were prepared as in (Dubois *et al.*, 2020a). Cells were scraped in ice-cold Phosphate-Buffered Saline (PBS), pelleted by centrifugation at 400 g for 5 min, lysed in Buffer A (50 mM HEPES pH 7.5, 10 mM KCl, 1.5 mM MgCl2, 340 mM

sucrose, 10% glycerol, 1 mM DTT and protease inhibitor cocktail from Roche) and incubated for 10 min at 4°C. Samples were centrifuged at 1,300 g for 5 min at 4°C and supernatants were discarded. Nuclear pellets were washed with Buffer A and subsequently lysed in solution B (3 mM EDTA, 0.2 mM EGTA, 1 mM DTT, and protease inhibitor cocktail). After incubation for 30 min at 4°C, samples were centrifuged at 1,700 g for 5 min at 4°C and supernatants were discarded. Chromatin pellets were washed with solution B, resuspended in Buffer C (50 mM Tris–HCl pH 8.0, 1 mM MgCl2, and 83 U/µl benzonase) and incubated for 20 min at 4°C. Laemmli buffer 6× was added before loading for Western immunoblotting.

Western blot assays

Protein extraction and western blotting were performed as described in (Dubois *et al.*, 2020a). Protein concentrations were determined using the PierceTM BCA protein assay kit (Thermo scientific). Then, 20 µg of proteins were separated by 10% SDS-PAGE and immunodetected by Western immunoblotting using the primary antibodies listed in the Table S6. Primary antibodies were detected using HRP-conjugated secondary antibodies (Sigma-Aldrich). Images were acquired using the iBright^{TM} CL1500 Imaging System (Thermo Fisher Scientific).

Statistical analyses

Statistical analyses were performed using the Prism software (GraphPad, San Diego, CA) and R (R_Core_Team, 2015). The specific tests and corrections for multiple testing which were used as well as the number of mice or independent biological replicates are indicated in the figure legends. Two-sided tests were used unless specified in the figure legends. All bar graphs show means ± SD (standard deviations). Box plots are composed of a box from the 25th to the 75th percentile with the median as a line. Unless specified in the

figure legend, whiskers extent to the most extreme data point which is no more than 1.5 times the interquartile range from the box.

ACKNOWLEDGMENTS

The authors thank Drs Wang and Liu (Vanderbilt University Medical Center, Nashville, TN, USA) for providing the summit coordinates of active mouse liver promoters and Drs Ninon Very N and Marie Bobowski-Gerard (Inserm U1011, Univ. Lille) for technical assistance.

Financial support: This work was supported by the Agence Nationale de la Recherche (ANR) grants "HSCreg" (ANR-21-CE14-0032), "MEdicAL" (ANR-21-CE17-0016) and "European Genomic Institute for Diabetes" E.G.I.D (ANR-10-LABX-0046), a French State fund managed by ANR under the frame program Investissements d'Avenir I-SITE ULNE / ANR-16-IDEX-0004 ULNE as well as by Fondation Recherche Médicale (FRM grants EQU202203014645).

DISCLOSURES

The authors declare no competing interests.

AUTHOR CONTRIBUTIONS

Conceptualization: JD-C, CG, KG, LD, BS, PL, JE; validation: JD-C, CG; formal analysis: JD-C, CG, JE; investigation: JD-C, CG, AB, CB, VD, LG, MF, GM; resources: KG, LD; data curation: JD-C, CG, JE; writing—review & editing: JD-C, CG and JE with inputs from co-authors; visualization: JD-C, CG, JE; project administration: BS, PL, JE; funding acquisition: BS, PL, JE.

DATA AVAILABILITY

Transcriptomics data generated in this study have been deposited into the Gene Expression Omnibus (GEO) database and are available under accession numbers GSE216278 and GSE218724. The following secure tokens allow review of these GEO records: olclmskcbdsxdij and gfwfakaezxoppsr, respectively.

REFERENCES

Afgan E, Baker D, Batut B, van den Beek M, Bouvier D, Cech M, Chilton J, Clements D, Coraor N, Gruning BA *et al* (2018) The Galaxy platform for accessible, reproducible and collaborative biomedical analyses: 2018 update. *Nucleic Acids Res* 46: W537-W544

Almeida N, Chung MWH, Drudi EM, Engquist EN, Hamrud E, Isaacson A, Tsang VSK, Watt FM, Spagnoli FM (2021) Employing core regulatory circuits to define cell identity. *EMBO J*: e106785

Amemiya HM, Kundaje A, Boyle AP (2019) The ENCODE Blacklist: Identification of Problematic Regions of the Genome. *Sci Rep* 9: 9354

Anders S, Pyl PT, Huber W (2015) HTSeq--a Python framework to work with high-throughput sequencing data. *Bioinformatics* 31: 166-169

Arendt D, Musser JM, Baker CVH, Bergman A, Cepko C, Erwin DH, Pavlicev M, Schlosser G, Widder S, Laubichler MD *et al* (2016) The origin and evolution of cell types. *Nat Rev Genet* 17: 744-757

Argemi J, Latasa MU, Atkinson SR, Blokhin IO, Massey V, Gue JP, Cabezas J, Lozano JJ, Van Booven D, Bell A *et al* (2019) Defective HNF4alpha-dependent gene expression as a driver of hepatocellular failure in alcoholic hepatitis. *Nature Communications* 10

Barrett T, Wilhite SE, Ledoux P, Evangelista C, Kim IF, Tomashevsky M, Marshall KA, Phillippy KH, Sherman PM, Holko M *et al* (2013) NCBI GEO: archive for functional genomics data sets--update. *Nucleic Acids Res* 41: D991-995

Bedward M, Keith D, Pressey R (1992) Homogeneity analysis: Assessing the utility of classifications and maps of natural resources. *Australian Journal of Ecology* 17: 133-139

Benayoun BA, Pollina EA, Ucar D, Mahmoudi S, Karra K, Wong ED, Devarajan K, Daugherty AC, Kundaje AB, Mancini E *et al* (2014) H3K4me3 breadth is linked to cell identity and transcriptional consistency. *Cell* 158: 673-688

Berasain C, Arechederra M, Argemi J, Fernandez-Barrena MG, Avila MA (2022) Loss of liver function in chronic liver disease: an identity crisis. *J Hepatol*

Bideyan L, Nagari R, Tontonoz P (2021) Hepatic transcriptional responses to fasting and feeding. *Genes Dev* 35: 635-657

Billon C, Canaple L, Fleury S, Deloire A, Beylot M, Dombrowicz D, Del Carmine P, Samarut J, Gauthier K (2014) TRalpha protects against atherosclerosis in male mice: identification of a novel anti-inflammatory property for TRalpha in mice. *Endocrinology* 155: 2735-2745

Bobowski-Gerard M, Boulet C, Zummo FP, Dubois-Chevalier J, Gheeraert C, Bou Saleh M, Strub JM, Farce A, Ploton M, Guille L *et al* (2022) Functional genomics uncovers the transcription factor BNC2 as required for myofibroblastic activation in fibrosis. *Nat Commun* 13: 5324

Bou Saleh M, Louvet A, Ntandja-Wandji LC, Boleslawski E, Gnemmi V, Lassailly G, Truant S, Maggiotto F, Ningarhari M, Artru F *et al* (2021) Loss of hepatocyte identity following aberrant YAP activation: a key mechanism in alcoholic hepatitis. *J Hepatol* 75: 912-923

Boyer LA, Lee TI, Cole MF, Johnstone SE, Levine SS, Zucker JP, Guenther MG, Kumar RM, Murray HL, Jenner RG *et al* (2005) Core transcriptional regulatory circuitry in human embryonic stem cells. *Cell* 122: 947-956

Chao J, Zhao S, Sun H (2020) Dedifferentiation of hepatocellular carcinoma: molecular mechanisms and therapeutic implications. *Am J Transl Res* 12: 2099-2109

Chen J, Xu H, Aronow BJ, Jegga AG (2007) Improved human disease candidate gene prioritization using mouse phenotype. *BMC Bioinformatics* 8: 392

Chen K, Chen Z, Wu D, Zhang L, Lin X, Su J, Rodriguez B, Xi Y, Xia Z, Chen X *et al* (2015) Broad H3K4me3 is associated with increased transcription elongation and enhancer activity at tumor-suppressor genes. *Nat Genet* 47: 1149-1157

Chubb JR, Ford HZ, Antolović V (2021) Distributed and centralized control during differentiation. *Developmental Cell* 56: 2142-2144

D'Alessio Ana C, Fan Zi P, Wert Katherine J, Baranov P, Cohen Malkiel A, Saini Janmeet S, Cohick E, Charniga C, Dadon D, Hannett Nancy M *et al* (2015) A Systematic Approach to Identify Candidate Transcription Factors that Control Cell Identity. *Stem Cell Reports* 5: 763-775

Dalgaard K, Landgraf K, Heyne S, Lempradl A, Longinotto J, Gossens K, Ruf M, Orthofer M, Strogantsev R, Selvaraj M *et al* (2016) Trim28 Haploinsufficiency Triggers Bi-stable Epigenetic Obesity. *Cell* 164: 353-364

Del Campo JA, Gallego P, Grande L (2018) Role of inflammatory response in liver diseases: Therapeutic strategies. *World J Hepatol* 10: 1-7

Dubois-Chevalier J, Dubois V, Dehondt H, Mazrooei P, Mazuy C, Sérandour AA, Gheeraert C, Guillaume P, Baugé E, Derudas B *et al* (2017a) The logic of transcriptional regulator recruitment architecture at cis-regulatory modules controlling liver functions. *Genome Res* 27: 985-996

Dubois-Chevalier J, Dubois V, Staels B, Lefebvre P, Eeckhoute J (2020) Perspectives on the use of super-enhancers as a defining feature of cell/tissue-identity genes. *Epigenomics*

Dubois-Chevalier J, Mazrooei P, Lupien M, Staels B, Lefebvre P, Eeckhoute J (2017b) Organizing combinatorial transcription factor recruitment at cis-regulatory modules. *Transcription*: 1-7

Dubois V, Gheeraert C, Vankrunkelsven W, Dubois-Chevalier J, Dehondt H, Bobowski-Gerard M, Vinod M, Zummo FP, Güiza F, Ploton M *et al* (2020a) Endoplasmic reticulum stress actively suppresses hepatic molecular identity in damaged liver. *Mol Syst Biol* 16: e9156

Dubois V, Staels B, Lefebvre P, Verzi MP, Eeckhoute J (2020b) Control of Cell Identity by the Nuclear Receptor HNF4 in Organ Pathophysiology. *Cells* 9: 2185

Duncan AW, Taylor MH, Hickey RD, Newell AEH, Lenzi ML, Olson SB, Finegold MJ, Grompe M (2010) The ploidy conveyor of mature hepatocytes as a source of genetic variation. *Nature* 467: 707

Frankish A, Diekhans M, Ferreira AM, Johnson R, Jungreis I, Loveland J, Mudge JM, Sisu C, Wright J, Armstrong J *et al* (2018) GENCODE reference annotation for the human and mouse genomes. *Nucleic Acids Res*

Freese NH, Norris DC, Loraine AE (2016) Integrated genome browser: visual analytics platform for genomics. *Bioinformatics* 32: 2089-2095

Gao J, Aksoy BA, Dogrusoz U, Dresdner G, Gross B, Sumer SO, Sun Y, Jacobsen A, Sinha R, Larsson E *et al* (2013) Integrative analysis of complex cancer genomics and clinical profiles using the cBioPortal. *Sci Signal* 6: pl1

Gartner K (1990) A third component causing random variability beside environment and genotype. A reason for the limited success of a 30 year long effort to standardize laboratory animals? *Lab Anim* 24: 71-77

González-Blas CB, Matetovici I, Hillen H, Taskiran II, Vandepoel R, Christiaens V, Sansores-García L, Verboven E, Hulselmans G, Poovathingal S *et al* (2022) Enhancer grammar of liver cell types and hepatocyte zonation states. *bioRxiv*: 2022.2012.2008.519575

Gunewardena S, Huck I, Walesky C, Robarts D, Weinman S, Apte U (2022) Progressive loss of HNF4alpha activity in chronic liver diseases in humans. *Hepatology*

Hahsler M, Gruen B, Hornik K (2005) arules – A Computational Environment for Mining Association Rules and Frequent Item Sets. *Journal of Statistical Software* 14: 1-25

Hatziagelaki E, Paschou SA, Schon M, Psaltopoulou T, Roden M (2022) NAFLD and thyroid function: pathophysiological and therapeutic considerations. *Trends Endocrinol Metab*

Hnisz D, Abraham BJ, Lee TI, Lau A, Saint-Andre V, Sigova AA, Hoke HA, Young RA (2013) Super-enhancers in the control of cell identity and disease. *Cell* 155: 934-947

Howe KL, Achuthan P, Allen J, Allen J, Alvarez-Jarreta J, Amode MR, Armean IM, Azov AG, Bennett R, Bhai J *et al* (2021) Ensembl 2021. *Nucleic Acids Res* 49: D884-D891

Hunter AL, Pelekanou CE, Adamson A, Downton P, Barron NJ, Cornfield T, Poolman TM, Humphreys N, Cunningham PS, Hodson L *et al* (2020) Nuclear receptor REVERBalpha is a state-dependent regulator of liver energy metabolism. *Proc Natl Acad Sci U S A*

Hyun J, Sun Z, Ahmadi AR, Bangru S, Chembazhi UV, Du K, Chen T, Tsukamoto H, Rusyn I, Kalsotra A *et al* (2020) Epithelial splicing regulatory protein 2-mediated alternative splicing reprograms hepatocytes in severe alcoholic hepatitis. *J Clin Invest*

Kaimal V, Bardes EE, Tabar SC, Jegga AG, Aronow BJ (2010) ToppCluster: a multiple gene list feature analyzer for comparative enrichment clustering and network-based dissection of biological systems. *Nucleic Acids Res* 38: W96-102

Kim D, Paggi JM, Park C, Bennett C, Salzberg SL (2019) Graph-based genome alignment and genotyping with HISAT2 and HISAT-genotype. *Nat Biotechnol* 37: 907-915

Kowalik MA, Puliga E, Cabras L, Sulas P, Petrelli A, Perra A, Ledda-Columbano GM, Morandi A, Merlin S, Orru C *et al* (2020) Thyroid hormone inhibits hepatocellular carcinoma progression via induction of differentiation and metabolic reprogramming. *J Hepatol* 72: 1159-1169

Kryuchkova-Mostacci N, Robinson-Rechavi M (2017) A benchmark of gene expression tissue-specificity metrics. *Brief Bioinform* 18: 205-214

Kyrmizi I, Hatzis P, Katrakili N, Tronche F, Gonzalez FJ, Talianidis I (2006) Plasticity and expanding complexity of the hepatic transcription factor network during liver development. *Genes Dev* 20: 2293-2305

Lê S, Josse J, Husson F (2008) FactoMineR: An R Package for Multivariate Analysis. *Journal of Statistical Software* 25: 1-18

Leek JT, Johnson WE, Parker HS, E.J. F, Jaffe AE, Zhang Y, Storey JD, Torres LC (2022) sva: Surrogate Variable Analysis. *R package version 3440*

Liang B, Zhou Y, Qian M, Xu M, Wang J, Zhang Y, Song X, Wang H, Lin S, Ren C *et al* (2021) TBX3 functions as a tumor suppressor downstream of activated CTNNB1 mutants during hepatocarcinogenesis. *J Hepatol* 75: 120-131

Lin Z, Xia S, Liang Y, Ji L, Pan Y, Jiang S, Wan Z, Tao L, Chen J, Lin C *et al* (2020) LXR activation potentiates sorafenib sensitivity in HCC by activating microRNA-378a transcription. *Theranostics* 10: 8834-8850

Liu R, Holik AZ, Su S, Jansz N, Chen K, Leong HS, Blewitt ME, Asselin-Labat ML, Smyth GK, Ritchie ME (2015) Why weight? Modelling sample and observational level variability improves power in RNA-seq analyses. *Nucleic Acids Res* 43: e97

Lizio M, Harshbarger J, Shimoji H, Severin J, Kasukawa T, Sahin S, Abugessaisa I, Fukuda S, Hori F, Ishikawa-Kato S *et al* (2015) Gateways to the FANTOM5 promoter level mammalian expression atlas. *Genome Biol* 16: 22

Lo JH, Edwards M, Langerman J, Sridharan R, Plath K, Smale ST (2022) Oct4:Sox2 binding is essential for establishing but not maintaining active and silent states of dynamically regulated genes in pluripotent cells. *Genes Dev* 36: 1079-1095

Loft A, Alfaro AJ, Schmidt SF, Pedersen FB, Terkelsen MK, Puglia M, Chow KK, Feuchtinger A, Troullinaki M, Maida A *et al* (2021) Liver-fibrosis-activated transcriptional networks govern hepatocyte reprogramming and intra-hepatic communication. *Cell Metab*

Loven J, Hoke HA, Lin CY, Lau A, Orlando DA, Vakoc CR, Bradner JE, Lee TI, Young RA (2013) Selective inhibition of tumor oncogenes by disruption of super-enhancers. *Cell* 153: 320-334

Meng H, Gonzales NM, Lonard DM, Putluri N, Zhu B, Dacso CC, York B, O'Malley BW (2020) XBP1 links the 12-hour clock to NAFLD and regulation of membrane fluidity and lipid homeostasis. *Nat Commun* 11: 6215

Mittnenzweig M, Mayshar Y, Cheng S, Ben-Yair R, Hadas R, Rais Y, Chomsky E, Reines N, Uzonyi A, Lumerman L *et al* (2021) A single-embryo, single-cell time-resolved model for mouse gastrulation. *Cell* 184: 2825-2842 e2822

Mukherji A, Bailey SM, Staels B, Baumert TF (2019) The circadian clock and liver function in health and disease. *J Hepatol*

Nielsen CB, Younesy H, O'Geen H, Xu X, Jackson AR, Milosavljevic A, Wang T, Costello JF, Hirst M, Farnham PJ *et al* (2012) Spark: a navigational paradigm for genomic data exploration. *Genome Res* 22: 2262-2269

Pan Y, Ballance H, Meng H, Gonzalez N, Kim SM, Abdurehman L, York B, Chen X, Schnytzer Y, Levy O *et al* (2020) 12-h clock regulation of genetic information flow by XBP1s. *PLoS Biol* 18: e3000580

Papadakis M, Tsagris M, Dimitriadis M, Fafalios S, Tsamardinos I, Fasiolo M, Borboudakis G, Burkardt J, Zou C, Lakiotaki K *et al* (2022) Rfast: A Collection of Efficient and Extremely Fast R Functions. R package version 2.0.6, <https://CRAN.R-project.org/package=Rfast>.

Paquette MA, Dong H, Gagne R, Williams A, Malowany M, Wade MG, Yauk CL (2011) Thyroid hormone-regulated gene expression in juvenile mouse liver: identification of thyroid response elements using microarray profiling and in silico analyses. *BMC Genomics* 12: 634

Paris J, Henderson NC (2022) Liver zonation, revisited. *Hepatology*

Pekowska A, Benoukraf T, Ferrier P, Spicuglia S (2010) A unique H3K4me2 profile marks tissue-specific gene regulation. *Genome Res* 20: 1493-1502

Pohl A, Beato M (2014) bwtool: a tool for bigWig files. *Bioinformatics* 30: 1618-1619

Quinlan AR, Hall IM (2010) BEDTools: a flexible suite of utilities for comparing genomic features. *Bioinformatics* 26: 841-842

R_Core_Team (2015) R: A language and environment for statistical computing. *R Foundation for Statistical Computing*

Reizel Y, Morgan A, Gao L, Lan Y, Manduchi E, Waite EL, Wang AW, Wells A, Kaestner KH (2020) Collapse of the hepatic gene regulatory network in the absence of FoxA factors. *Genes Dev*

Ritchie ME, Phipson B, Wu D, Hu Y, Law CW, Shi W, Smyth GK (2015) limma powers differential expression analyses for RNA-sequencing and microarray studies. *Nucleic Acids Res* 43: e47

Robinson MD, McCarthy DJ, Smyth GK (2010) edgeR: a Bioconductor package for differential expression analysis of digital gene expression data. *Bioinformatics* 26: 139-140

Roh HC, Tsai LT, Lyubetskaya A, Tenen D, Kumari M, Rosen ED (2017) Simultaneous Transcriptional and Epigenomic Profiling from Specific Cell Types within Heterogeneous Tissues In Vivo. *Cell Rep* 18: 1048-1061

Russo-Savage L, Schulman IG (2021) Liver X receptors and liver physiology. *Biochim Biophys Acta Mol Basis Dis* 1867: 166121

Sarkans U, Fullgrabe A, Ali A, Athar A, Behrangi E, Diaz N, Fexova S, George N, Iqbal H, Kurri S *et al* (2021) From ArrayExpress to BioStudies. *Nucleic Acids Res* 49: D1502-D1506

Schippers IJ, Moshage H, Roelofsen H, Muller M, Heymans HS, Ruiters M, Kuipers F (1997a) Immortalized human hepatocytes as a tool for the study of hepatocytic (de-)differentiation. *Cell Biol Toxicol* 13: 375-386

Schippers IJ, Moshage H, Roelofsen H, Müller M, Heymans HSA, Ruiters M, Kuipers F (1997b) Immortalized human hepatocytes as a tool for the study of hepatocytic (de-)diȷerentiation. *Cell Biology andToxicology* 13: 375-386

Schmidt D, Wilson MD, Ballester B, Schwalie PC, Brown GD, Marshall A, Kutter C, Watt S, Martinez-Jimenez CP, Mackay S *et al* (2010) Five-vertebrate ChIP-seq Reveals the Evolutionary Dynamics of Transcription Factor Binding *Science* 328: 1036-1040

Shen Y, Yue F, McCleary DF, Ye Z, Edsall L, Kuan S, Wagner U, Dixon J, Lee L, Lobanenkov VV *et al* (2012) A map of the cis-regulatory sequences in the mouse genome. *Nature* 488: 116-120

Singh BK, Sinha RA, Tripathi M, Mendoza A, Ohba K, Sy JAC, Xie SY, Zhou J, Ho JP, Chang CY *et al* (2018) Thyroid hormone receptor and ERRalpha coordinately regulate mitochondrial fission, mitophagy, biogenesis, and function. *Sci Signal* 11

Smith CL, Goldsmith CA, Eppig JT (2005) The Mammalian Phenotype Ontology as a tool for annotating, analyzing and comparing phenotypic information. *Genome Biol* 6: R7

Sommars MA, Ramachandran K, Senagolage MD, Futtner CR, Germain DM, Allred AL, Omura Y, Bederman IR, Barish GD (2019) Dynamic repression by BCL6 controls the genome-wide liver response to fasting and steatosis. *eLife* 8

Sun J, Wang B, Liu Y, Zhang L, Ma A, Yang Z, Ji Y, Liu Y (2014) Transcription factor KLF9 suppresses the growth of hepatocellular carcinoma cells in vivo and positively regulates p53 expression. *Cancer Lett* 355: 25-33

Tachmatzidi EC, Galanopoulou O, Talianidis I (2021) Transcription Control of Liver Development. *Cells* 10

Tan HW, Leung CO, Chan KK, Ho DW, Leung MS, Wong CM, Ng IO, Lo RC (2019) Deregulated GATA6 modulates stem cell-like properties and metabolic phenotype in hepatocellular carcinoma. *Int J Cancer* 145: 1860-1873

Tang Q, Zeng M, Chen L, Fu N (2022) Targeting Thyroid Hormone/Thyroid Hormone Receptor Axis: An Attractive Therapy Strategy in Liver Diseases. *Front Pharmacol* 13: 871100

Tuttle AH, Philip VM, Chesler EJ, Mogil JS (2018) Comparing phenotypic variation between inbred and outbred mice. *Nat Methods* 15: 994-996

Vandel J, Gheeraert C, Staels B, Eeckhoute J, Lefebvre P, Dubois-Chevalier J (2020) GIANT: galaxy-based tool for interactive analysis of transcriptomic data. *Sci Rep* 10: 19835

Vazquez Salgado AM, Preziosi ME, Yin D, Holczbauer A, Zahm AM, Erez N, Kieckhaefer J, Ackerman D, Gade TP, Kaestner KH *et al* (2022) In Vivo Screen Identifies Liver X Receptor Alpha Agonism Potentiates Sorafenib Killing of Hepatocellular Carcinoma. *Gastro Hep Adv* 1: 905-908

Wang J, Zhao Y, Zhou X, Hiebert SW, Liu Q, Shyr Y (2018) Nascent RNA sequencing analysis provides insights into enhancer-mediated gene regulation. *BMC Genomics* 19: 633

Warnes GR, Bolker B, Bonebakker L, Gentleman R, Huber W, Liaw WHA, Lumley T, Maechler M, Magnusson A, Moeller S *et al* (2022) gplots: Various R Programming Tools for Plotting Data. R package version 3.1.3.

Wehrens R, Buydens L (2007) Self- and Super-organizing Maps in R: The kohonen Package. *J Stat Softw* 21

Whyte WA, Orlando DA, Hnisz D, Abraham BJ, Lin CY, Kagey MH, Rahl PB, Lee TI, Young RA (2013) Master transcription factors and mediator establish super-enhancers at key cell identity genes. *Cell* 153: 307-319

Wickham H (2016) ggplot2: Elegant Graphics for Data Analysis. *Springer-Verlag New York*

Wilkinson AC, Nakauchi H, Gottgens B (2017) Mammalian Transcription Factor Networks: Recent Advances in Interrogating Biological Complexity. *Cell Syst* 5: 319-331

Wu C, Jin X, Tsueng G, Afrasiabi C, Su AI (2016) BioGPS: building your own mash-up of gene annotations and expression profiles. *Nucleic Acids Res* 44: D313-316

Yang CH, Fagnocchi L, Apostle S, Wegert V, Casani-Galdon S, Landgraf K, Panzeri I, Dror E, Heyne S, Worpel T *et al* (2022) Independent phenotypic plasticity axes define distinct obesity sub-types. *Nat Metab* 4: 1150-1165

Yates AD, Achuthan P, Akanni W, Allen J, Allen J, Alvarez-Jarreta J, Amode MR, Armean IM, Azov AG, Bennett R *et al* (2020) Ensembl 2020. *Nucleic Acids Res* 48: D682-D688

Yuan C, Lin JZ, Sieglaff DH, Ayers SD, Denoto-Reynolds F, Baxter JD, Webb P (2012) Identical gene regulation patterns of T3 and selective thyroid hormone receptor modulator GC-1. *Endocrinology* 153: 501-511

Zhang HM, Liu T, Liu CJ, Song S, Zhang X, Liu W, Jia H, Xue Y, Guo AY (2015) AnimalTFDB 2.0: a resource for expression, prediction and functional study of animal transcription factors. *Nucleic Acids Res* 43: D76-81

Zhang Y, Liu T, Meyer CA, Eeckhoute J, Johnson DS, Bernstein BE, Nusbaum C, Myers RM, Brown M, Li W *et al* (2008) Model-based analysis of ChIP-Seq (MACS). *Genome Biol* 9: R137

Zhou Q, Liu M, Xia X, Gong T, Feng J, Liu W, Liu Y, Zhen B, Wang Y, Ding C *et al* (2017) A mouse tissue transcription factor atlas. *Nat Commun* 8: 15089

Figure legends:

Fig.1. Promoter-centric mining of the hepatic TF network using ProTFnet.

A) The cistromes of 8 Hep-ID TFs (CEBPA, FOXA2, HNF4A, NR1H4, NR5A2, ONECUT1, PPARA, PROX1; Table S2) were used to define the percentage of those TFs binding to Hep-ID TF (n=13) or non-Hep-ID TF (Control TF genes; n=13) encoding gene promoters. The control group used was selected for providing data representative of those obtained with 1000 reiterations of this analysis. Wilcoxon rank sum test with continuity correction was used to assess statistical significance. *$p<0.05$. **B)** Overview of the ProTFnet strategy implemented in this study where (identity) TF binding to TF-encoding gene promoters is monitored and subsequently used to define distinct clusters of promoters through SOM and hierarchical clustering. Clusters are subsequently characterized using multi-omics (cistromic, epigenomic and transcriptomic) data mining to explore the complexity of the identity TF network. **C)** Planar view of the toroidal map issued from the SOM analysis was used here to display clusters A-G and hereafter to visualize different features of these clusters (panels D-E and Fig.S3E). The dendrogram issued from the hierarchical clustering analysis is shown on the right. **D)** The map issued from the SOM analyses was used to show the average number of co-recruited TFs at gene promoters contained in individual cells. Bold orange lines indicate the borders of clusters A-G. **E)** The map issued from the SOM analyses was used to show the average ChIP-seq signal for mouse liver H3K27ac at gene promoters contained in individual cells. Bold black lines indicate the borders of clusters A-G. **F)** Heatmap showing the occurrence (percentage) of individual transcriptional regulators in the core co-recruitment nodes of clusters A-G, i.e. binding combinations found in at least 50% of the promoters of a given cluster. **G)** Heatmap displaying the distribution (percentage) of promoters for each one of clusters A-G into clusters 1-7, where promoters were grouped according to increasing hepatic activity score (Fig.S6). **H)** Enrichment for Hep-ID TF genes (Table S1) within the

different groups of TF gene promoters. Here, and in all subsequent analyses of the clusters A-G and 1-7 cross-comparison, groups containing less than 10 promoters were not displayed. **I)** The normalized cistromes of 8 Hep-ID TFs (see A) were used to define the median Hep-ID TF ChIP-seq signal at promoters found in the different groups. **J)** Principal component analysis (PCA) of TF gene expression in mouse (n=39) and human (n=126) primary cell-types (see Materials and Methods). Individual TFs are displayed as dots projected on the first 2 components and the 3 main clusters issued from hierarchical clustering are shown and labelled as UBQ (ubiquitous), CTE (cell-type enriched) and CTS (cell-type specific) (Fig.S8). **K)** The data from panel J were used to selectively display TF genes from cluster G.

Fig.2. Identification and characterization of Hep-ID^{CONNECT} TFs.

A) The CTE/UBQ TFs from cluster G (Fig.1K) were plotted based on their expression in mouse primary hepatocytes (MPH) when compared to other primary mouse cell-types (n=38). For each individual TF, cells were first ranked according to decreasing gene expression and the rank of MPH was plotted on the *x* axis (i.e. rank 1 indicates highest expression is in MPH). Second, expression in MPH was divided by the average expression in all other primary cells and plotted on the *y* axis as $\log_2$ fold difference. Hep-ID^{CONNECT} TF-encoding genes were defined as those preferentially expressed in MPH (rank ≤10 and FC>0). For comparison, Hep-ID TF genes were plotted in an additional box on the right of the one highlighting Hep-ID^{CONNECT} TFs. **B-E)** Expression of Hep-ID, Hep-ID^{CONNECT} and remaining TF-encoding genes from cluster G (Others) was monitored in indicated transcriptomic data (Table S2). Box plots show $\log_2$ fold changes between MPH of *Hnf4a*$^{hep-/-}$ (*Hnf4a* KO) *versus* wild-type mice (B), adult *versus* newborn mouse livers (C), a meta-analysis of severe mouse liver injuries *versus* control livers (D; see Materials and Methods and Fig.S10) and microdissected hepatocytes from alcohol-related human liver cirrhosis (alcoholic steatohepatitis) *versus* control livers (E). Statistical significance was assessed using one-sided one-sample t-test with Benjamini-Hochberg correction for multiple testing to determine if the mean $\log_2$ FC was statistically lower (B, D, E) or higher (C) than 0. *q<0.05. **F)** Distribution of H3K4me3 domain length at the TSS of Hep-ID, Hep-ID^{CONNECT} and remaining TF-encoding genes from cluster G (Others) as defined through broad peak calling on mouse liver H3K4me3 ChIP-seq data. Statistical difference between groups was defined using Kruskal-Wallis with Wilcoxon pairwise comparison tests followed by Benjamini-Hochberg correction for multiple testing correction. *q<0.05. **G)** Mouse phenotypes associated with Hep-ID, Hep-ID^{CONNECT} and remaining TF-encoding genes from cluster G (Others) were defined using ToppCluster. Dendrograms of hierarchical clustering are shown. ToppCluster uses

hypergeometric tests and Bonferroni correction. **H)** Enrichment for identity effector genes among the top 1000 transcriptionally dysregulated genes in the MPH/livers of indicated genetically deficient mice. Log_2 odds ratios were computed to compare the proportion of dysregulated versus non-dysregulated genes within identity effector genes or control non-TF-encoding genes. Then a two-sided Fisher exact test was performed to assess if the proportion of dysregulated genes was significatively different within the identity and control gene groups with Benjamini-Hochberg correction. *q<0.05. **I)** Binding of indicated Hep-ID and Hep-ID^{CONNECT} TFs to the promoter of identity effector genes and a control group of non-TF-encoding genes of similar size (n=424) was monitored using mouse liver ChIP-seq data. A control group of non-TF-encoding genes (n=424) matched for their promoter mouse liver activity was also used (Fig.S13). The control groups used were selected for providing data representative of those obtained with 1000 reiterations of this analysis (see Materials and Methods; Fig.S13). The distribution of ChIP-seq signals is shown using box plots. Pairwise Wilcoxon Rank Sum Tests with Benjamini-Hochberg correction was used to define whether the binding at identity effector genes *versus* control genes was significantly different for each analyzed TF recruitment. *q<0.05. **J)** Correlation between Hep-ID TFs, Hep-ID^{CONNECT} TFs and CTCF recruitment, as judged through the mining of mouse liver ChIP-seq data, to identity effector genes. The dendrogram is issued from hierarchical clustering analysis.

Fig.3. Hep-ID^{CONNECT} TF binding to and regulation of Hep-ID TF encoding genes in basal conditions.

A) Binding of indicated Hep-ID and Hep-ID^{CONNECT} TFs to the promoter of Hep-ID TF genes and a control group of non-Hep-ID TF-encoding genes matched for their promoter activity (Fig.S14) of similar size (n=13) was monitored using mouse liver ChIP-seq data. The control group used was selected for providing data representative of those obtained with 1000 reiterations of this analysis (see Materials and Methods; Fig.S14). The distribution of ChIP-seq signals is shown using box plots. One-sided Wilcoxon rank sum tests with Benjamini-Hochberg correction was used to define whether the binding on Hep-ID TF gene promoters was greater than on control genes for each individual TF ChIP-seq dataset. *q<0.05. **B)** Transcriptional modulation of Hep-ID TFs and a control group of non-Hep-ID TF-encoding genes matched for their promoter activity (Fig.S14) of similar size (n=13) in mouse liver/MPH of mice deleted for the indicated Hep-ID or Hep-ID^{CONNECT} TF genes. The control group used was selected for providing data representative of those obtained with 1000 reiterations of this analysis (see Materials and Methods; Fig.S14). The distribution of $\log_2$ fold changes is shown using box plots. Wilcoxon rank sum tests with Benjamini-Hochberg correction was used to define whether transcriptional regulation of Hep-ID TF genes was different from that of the control genes for each individual transcriptomic dataset. *q<0.05. **C)** 12hr gene expression oscillation analyses in the mouse liver performed by Meng et al. (Meng *et al.*, 2020) from WT and *XBP1*$^{hep-/-}$ animals were used to identify XBP1-dependent oscillating expression patterns for Hep-ID TF genes (Table S3). **D)** Average gene expression levels of *Mlxipl* in the livers of WT and *XBP1*$^{hep-/-}$ mice across circadian time.

Fig.4. Resetting Hep-ID TF gene expression through Hep-ID^{CONNECT} TF activation in hepatocellular carcinoma.

A) Distribution of the spearman correlations between Hep-ID TF genes and individual Hep-ID^{CONNECT} TF genes in human HCC shown using box plots. Hep-ID^{CONNECT} TFs which have been ascribed with HCC suppressive functions are indicated on the right. **B)** Cistromes for 13 Hep-ID^{CONNECT} TFs in HepG2 cells were mined for binding to Hep-ID TF encoding genes. Peaks localized +/- 10 kilobases from transcriptional start sites were considered in these analyses**. C)** Transcriptional modulation of Hep-ID TFs and a control group of non-Hep-ID TF-encoding genes matched for their promoter activity (Fig.S14) of similar size (n=13) in Huh7 or HepG2 cells treated with GW3965, T3 or GC-1, respectively. The control group used was selected for providing data representative of those obtained with 1000 reiterations of this analysis (see Materials and Methods; Fig.S14). The distribution of $\log_2$ fold changes is shown using box plots. Wilcoxon rank sum tests with Benjamini-Hochberg correction was used to define whether transcriptional regulation of Hep-ID TF genes was different from that of the control genes for each individual transcriptomic dataset. *q<0.05. **D-F)** mRNA expression of the indicated genes was monitored using RT-qPCR in HepG2 cells treated with T3 or GC-1 for 24h or 96h. Bar graphs show mean ±SD of $\log_2$ fold changes in treated *versus* untreated HepG2 cells. For *Hnf4a*, the $\log_2$ fold change in the ratio of P1 over P2 promoter-derived isoforms is also shown. Gray dots show the results obtained from 3 independent biological replicates, each performed in technical triplicates. One-sample t-test with Benjamini-Hochberg correction for multiple testing was used to determine if the mean log2 FC was statistically different from 0. *q<0.05. **G)** Western blots assays performed using antibodies against the indicated proteins on extracts from HepG2 cells treated or not with T3 for 24h. Rep#1-3 indicates the 3 independent biological replicates analyzed. **H)** Modulation of Hep-ID TF gene expression in precancerous nodules compared to control rat livers and in liver nodules of rats treated with T3 compared to nodules of non-treated rats. A control group of non-Hep-ID TF-encoding genes matched for their promoter activity (Fig.S14) of similar size

(n=13) is also shown. The control group used was selected for providing data representative of those obtained with 1000 reiterations of this analysis (see Materials and Methods; Fig.S14). Box plots show the log_2 fold changes. Wilcoxon rank sum tests with Benjamini-Hochberg correction was used to define whether transcriptional regulation of Hep-ID TF genes was different from that of the control genes for each individual transcriptomic dataset. *q<0.05. **I)** Dot plots showing the transcriptional regulation of individual Hep-ID TF gene expression in precancerous nodules compared to control rat livers (left; Nodules/Control) and in liver nodules of rats treated with T3 compared to nodules of non-treated rats (right; Nodules+T3/Nodules). No data were recovered for *Onecut2*, *Prox1* and *Mlxipl*. **J)** Identity effector genes significantly downregulated in Nodules/Control (q<0.05) were split in 3 groups according to their log_2 fold changes (i.e. low, intermediate and high repression; pink boxes) and then monitored for induction in Nodules+T3/Nodules (green boxes). Statistical differences between the High repression and the other groups regarding the Nodules/Control comparison, on the one hand, or the Nodules+T3/Nodules comparison, on the other hand, were defined using Kruskal-Wallis with Wilcoxon pairwise comparison tests followed by Benjamini-Hochberg correction for multiple testing correction. *q<0.05.

Fig.5. Resetting Hep-ID TF gene expression through THRB activation in inflammation-induced hepatocyte dedifferentiation.

A) Experimental protocol for acute inflammation-induced loss of hepatocyte identity *in vivo*. Mice were injected with IL1B (IL1B; n=17), IL1B followed by T3 (IL1B+T3; n=30) or a control group (PBS; n=14). All livers were collected 6h after the initial injection.

B-D) mRNA expression of the indicated genes was monitored in mouse livers using RT-qPCR. Mice treated with IL1B+T3 were subdivided into tertiles (n=10) based on the mean expression of the *Dio1* and *Hectd3* genes and defined as low, intermediate or high T3

responsiveness groups (Low resp., Int. resp. and High resp., respectively). Fold change relative to the mean of the control (PBS) group is shown using box plots whose whiskers extend to the maximum and minimum values. Statistical differences between the High resp. and the other IL1B-treated groups were defined using Kruskal-Wallis with Wilcoxon pairwise comparison tests followed by Benjamini-Hochberg correction for multiple testing correction. *$q<0.05$.

Figure 6. Proposed model for the control of hepatocyte identity by an extended transcription factor network. Schematic summarizing the main findings of our study pointing to an extended hepatic TF identity network which includes THRB. See discussion for greater details.

Fig.1

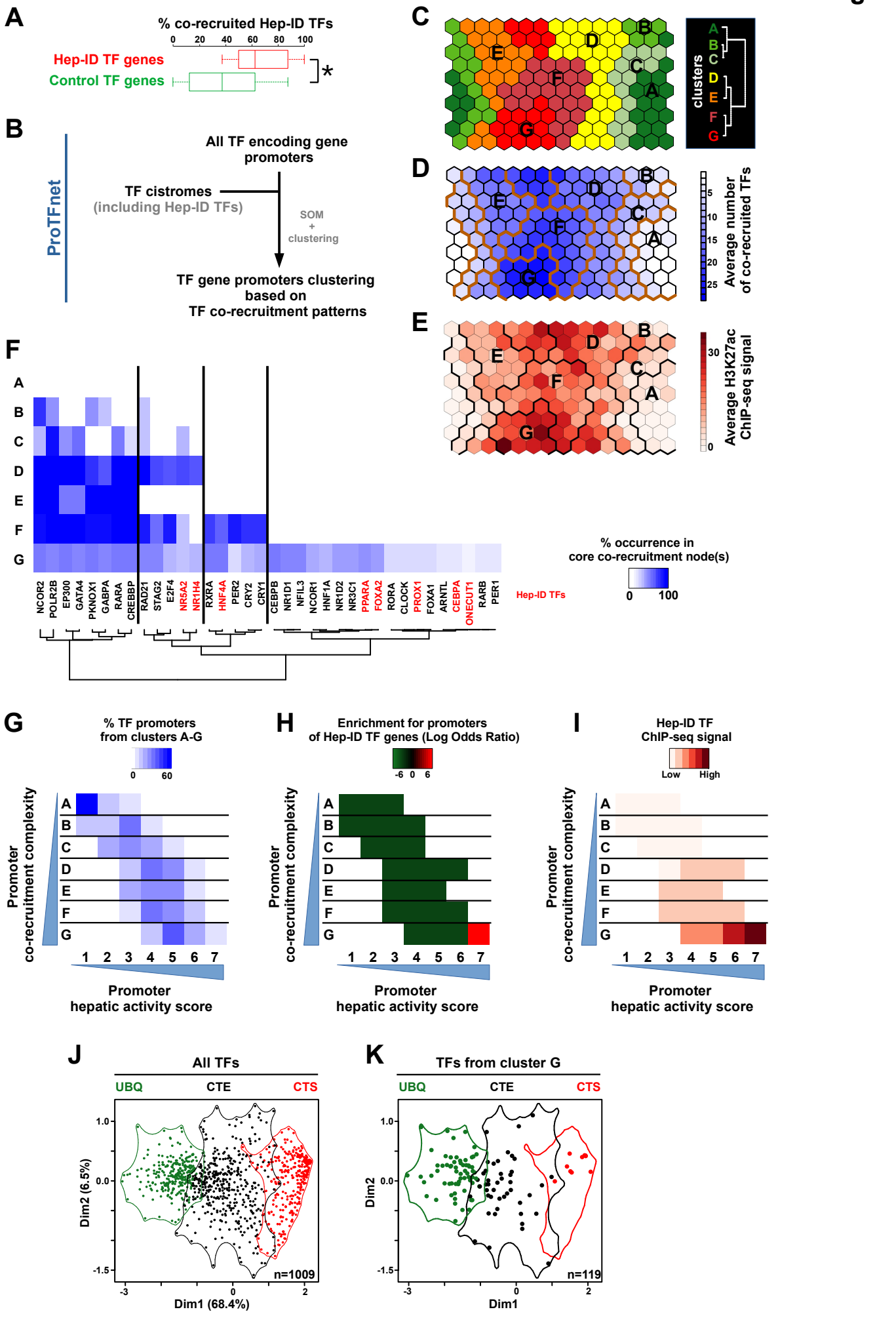
A
% co-recruited Hep-ID TFs
0 20 40 60 80 100
Hep-ID TF genes
Control TF genes
*
B
ProTFnet
All TF encoding gene promoters
TF cistromes (including Hep-ID TFs)
SOM + clustering
TF gene promoters clustering based on TF co-recruitment patterns
C
clusters
A B C D E F G
D
Average number of co-recruited TFs
5 10 15 20 25
E
Average H3K27ac ChIP-seq signal
30 0
F
A B C D E F G
NCOR2 POLR2B EP300 GATA4 PKNOX1 GABPA RARA CREBBP RAD21 STAG2 E2F4 NR5A2 NR1H4 RXRA HNF4A PER2 CRY2 CRY1 CEBPB NR1D1 NFIL3 NCOR1 HNF1A NR1D2 NR3C1 PPARA FOXA2 RORA CLOCK PROX1 FOXA1 ARNTL CEBPA ONECUT1 RARB PER1
Hep-ID TFs
% occurrence in core co-recruitment node(s)
0 100
G
% TF promoters from clusters A-G
0 60
Promoter co-recruitment complexity
Promoter hepatic activity score
H
Enrichment for promoters of Hep-ID TF genes (Log Odds Ratio)
-6 0 6
I
Hep-ID TF ChIP-seq signal
Low High
J
All TFs
UBQ CTE CTS
Dim2 (6.5%)
Dim1 (68.4%)
n=1009
K
TFs from cluster G
n=119

Fig.2

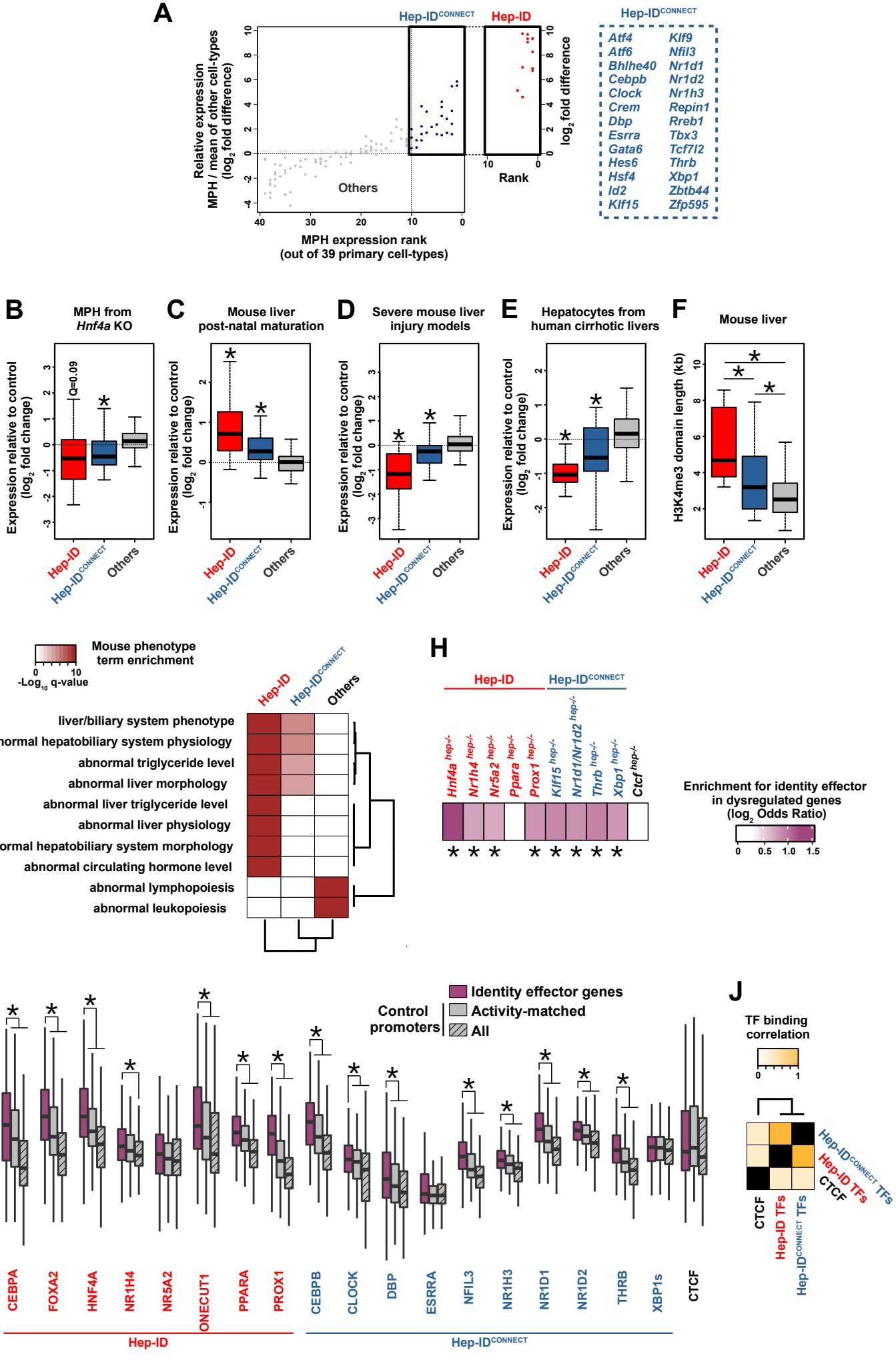
A
Hep-ID^CONNECT
Hep-ID
Relative expression MPH / mean of other cell-types (log2 fold difference)
log2 fold difference
Others
Rank
MPH expression rank (out of 39 primary cell-types)
Hep-ID^CONNECT
Atf4 Klf9
Atf6 Nfil3
Bhlhe40 Nr1d1
Cebpb Nr1d2
Clock Nr1h3
Crem Repin1
Dbp Rreb1
Esrra Tbx3
Gata6 Tcf7l2
Hes6 Thrb
Hsf4 Xbp1
Id2 Zbtb44
Klf15 Zfp595
B
MPH from Hnf4a KO
Q=0.09
C
Mouse liver post-natal maturation
D
Severe mouse liver injury models
E
Hepatocytes from human cirrhotic livers
F
Mouse liver
H3K4me3 domain length (kb)
Expression relative to control (log2 fold change)
Hep-ID
Hep-ID^CONNECT
Others
G
Mouse phenotype term enrichment
-Log10 q-value
liver/biliary system phenotype
abnormal hepatobiliary system physiology
abnormal triglyceride level
abnormal liver morphology
abnormal liver triglyceride level
abnormal liver physiology
abnormal hepatobiliary system morphology
abnormal circulating hormone level
abnormal lymphopoiesis
abnormal leukopoiesis
H
Hep-ID
Hep-ID^CONNECT
Hnf4a hep-/-
Nr1h4 hep-/-
Nr5a2 hep-/-
Ppara hep-/-
Prox1 hep-/-
Klf15 hep-/-
Nr1d1/Nr1d2 hep-/-
Thrb hep-/-
Xbp1 hep-/-
Ctcf hep-/-
Enrichment for identity effector in dysregulated genes (log2 Odds Ratio)
I
ChIP-seq signal relative to input (log2 fold enrichment)
Identity effector genes
Control promoters
Activity-matched
All
CEBPA FOXA2 HNF4A NR1H4 NR5A2 ONECUT1 PPARA PROX1 CEBPB CLOCK DBP ESRRA NFIL3 NR1H3 NR1D1 NR1D2 THRB XBP1s CTCF
Hep-ID
Hep-ID^CONNECT
J
TF binding correlation
Hep-ID^CONNECT TFs
Hep-ID TFs
CTCF

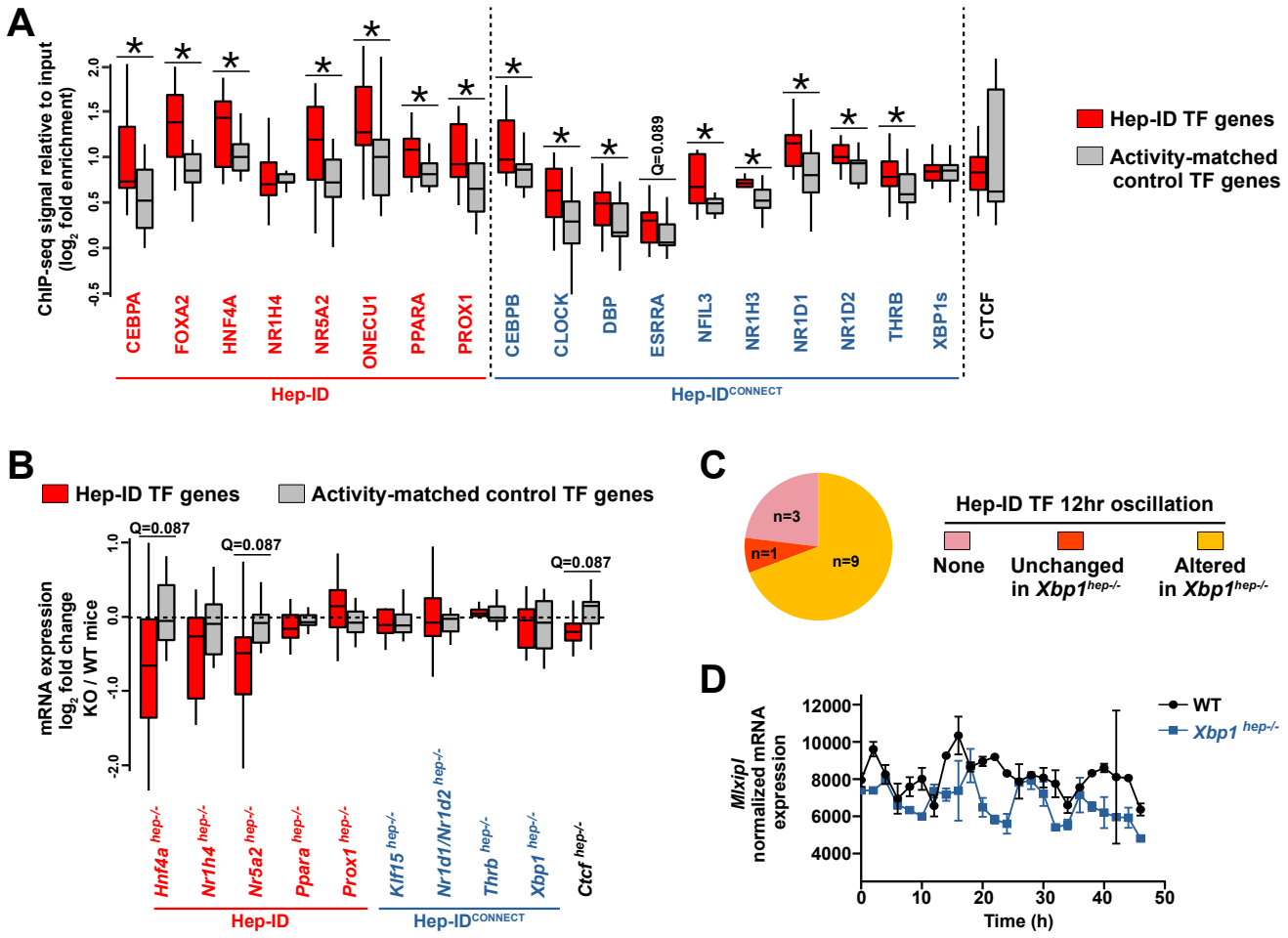
A
ChIP-seq signal relative to input
(log2 fold enrichment)
Hep-ID TF genes
Activity-matched control TF genes
CEBPA
FOXA2
HNF4A
NR1H4
NR5A2
ONECU1
PPARA
PROX1
CEBPB
CLOCK
DBP
ESRRA
NFIL3
NR1H3
NR1D1
NR1D2
THRB
XBP1s
CTCF
Q=0.089
Hep-ID
Hep-IDCONNECT
B
Hep-ID TF genes
Activity-matched control TF genes
mRNA expression
log2 fold change
KO / WT mice
Q=0.087
Q=0.087
Q=0.087
Hnf4a hep-/-
Nr1h4 hep-/-
Nr5a2 hep-/-
Ppara hep-/-
Prox1 hep-/-
Klf15 hep-/-
Nr1d1/Nr1d2 hep-/-
Thrb hep-/-
Xbp1 hep-/-
Ctcf hep-/-
Hep-ID
Hep-IDCONNECT
C
n=3
n=1
n=9
Hep-ID TF 12hr oscillation
None
Unchanged in Xbp1hep-/-
Altered in Xbp1hep-/-
D
Mlxipl normalized mRNA expression
WT
Xbp1 hep-/-
Time (h)

Fig.4

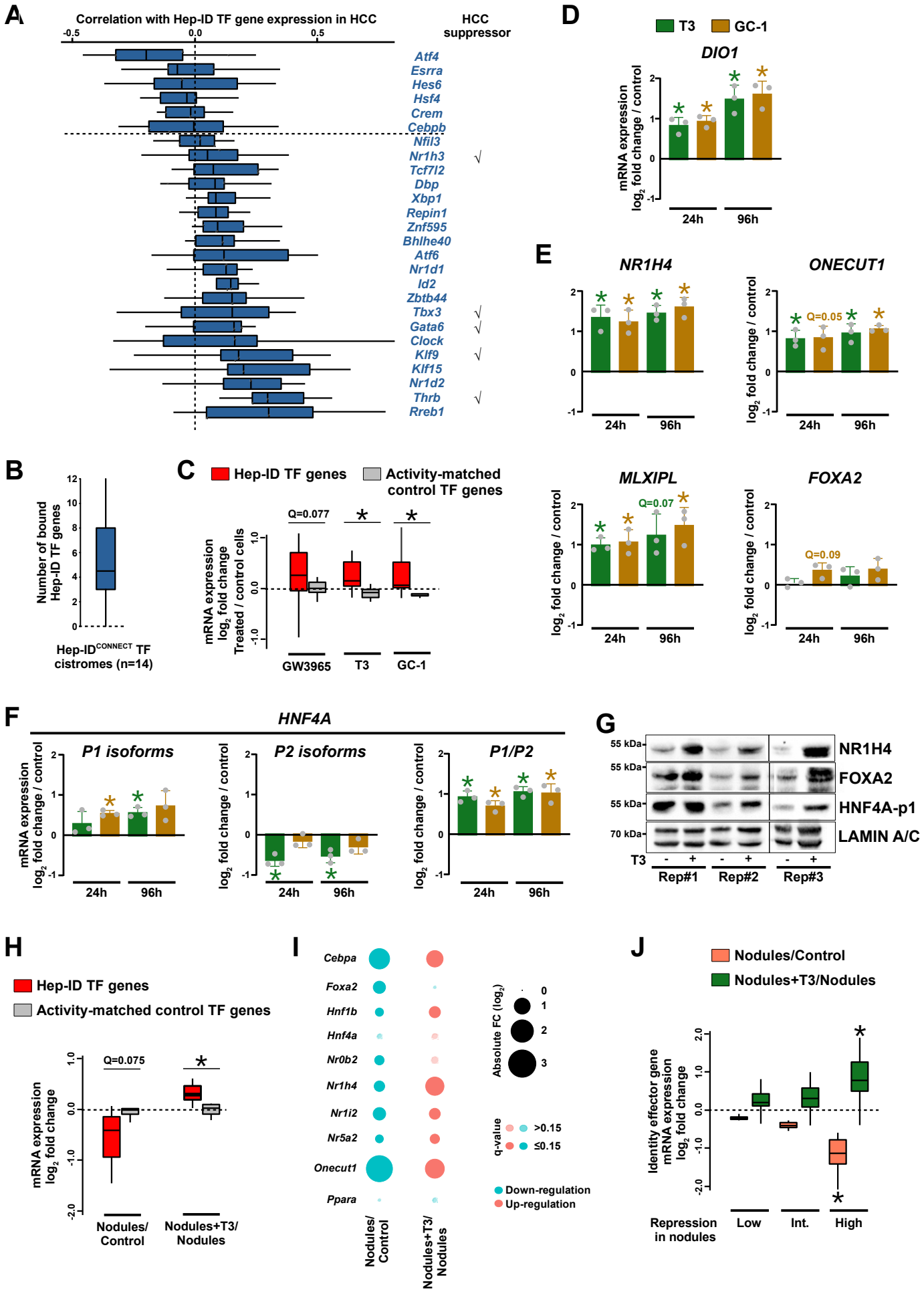
A
Correlation with Hep-ID TF gene expression in HCC
HCC suppressor
Atf4
Esrra
Hes6
Hsf4
Crem
Cebpb
Nfil3
Nr1h3
Tcf7l2
Dbp
Xbp1
Repin1
Znf595
Bhlhe40
Atf6
Nr1d1
Id2
Zbtb44
Tbx3
Gata6
Clock
Klf9
Klf15
Nr1d2
Thrb
Rreb1
B
Number of bound Hep-ID TF genes
Hep-ID CONNECT TF cistromes (n=14)
C
Hep-ID TF genes
Activity-matched control TF genes
Q=0.077
mRNA expression log2 fold change Treated / control cells
GW3965
T3
GC-1
D
T3
GC-1
DIO1
mRNA expression log2 fold change / control
24h
96h
E
NR1H4
ONECUT1
Q=0.05
MLXIPL
Q=0.07
FOXA2
Q=0.09
log2 fold change / control
F
HNF4A
P1 isoforms
P2 isoforms
P1/P2
G
55 kDa
70 kDa
NR1H4
FOXA2
HNF4A-p1
LAMIN A/C
T3
Rep#1
Rep#2
Rep#3
H
Hep-ID TF genes
Activity-matched control TF genes
Q=0.075
mRNA expression log2 fold change
Nodules/ Control
Nodules+T3/ Nodules
I
Cebpa
Foxa2
Hnf1b
Hnf4a
Nr0b2
Nr1h4
Nr1i2
Nr5a2
Onecut1
Ppara
Absolute FC (log2)
q-value
>0.15
≤0.15
Down-regulation
Up-regulation
J
Nodules/Control
Nodules+T3/Nodules
Identity effector gene mRNA expression log2 fold change
Repression in nodules
Low
Int.
High

Fig.5

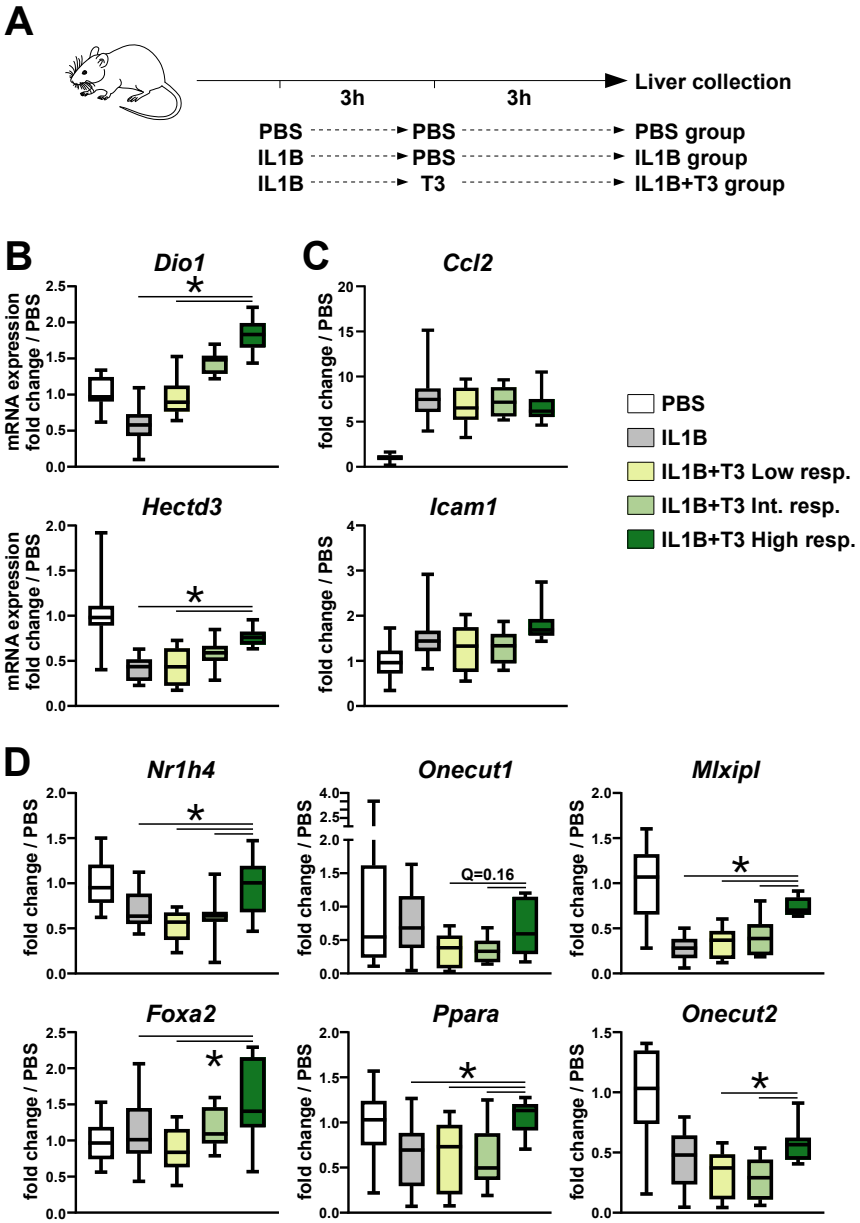
A
Liver collection
3h
3h
PBS
PBS
PBS group
IL1B
PBS
IL1B group
IL1B
T3
IL1B+T3 group
B
Dio1
mRNA expression
fold change / PBS
Hectd3
C
Ccl2
fold change / PBS
Icam1
PBS
IL1B
IL1B+T3 Low resp.
IL1B+T3 Int. resp.
IL1B+T3 High resp.
D
Nr1h4
Onecut1
Q=0.16
Mlxipl
Foxa2
Ppara
Onecut2

Fig.6

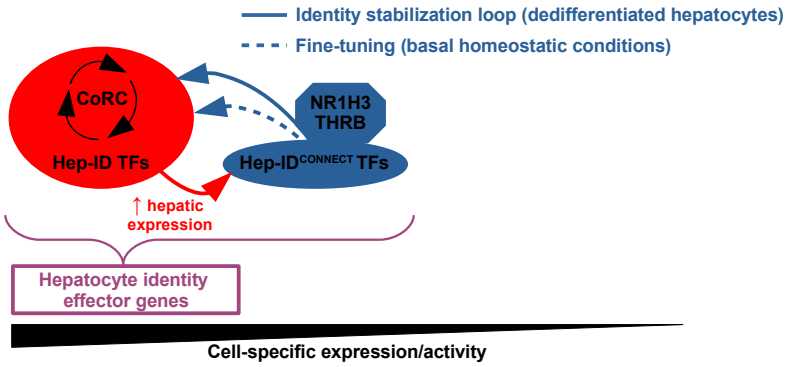
Identity stabilization loop (dedifferentiated hepatocytes)
Fine-tuning (basal homeostatic conditions)
CoRC
Hep-ID TFs
NR1H3
THRB
Hep-ID^CONNECT TFs
↑ hepatic expression
Hepatocyte identity effector genes
Cell-specific expression/activity